J. Fluid Mech. (2018), *vol.* 851, *pp.* 344–373.
doi:10.1017/jfm.2018.505

Unsteady thrust, lift and moment of a two-dimensional flapping thin airfoil in the presence of leading-edge vortices: a first approximation from linear potential theory

R. Fernandez-Feria[1],† and J. Alaminos-Quesada[1]

[1]Fluid Mechanics, Universidad de Málaga, Andalucía Tech, Dr Ortiz Ramos s/n, 29071 Málaga, Spain

(Received 4 December 2017; revised 25 April 2018; accepted 16 June 2018;
first published online 20 July 2018)

The effect of a leading-edge vortex (LEV) on the lift, thrust and moment of a two-dimensional heaving and pitching thin airfoil is analysed within the unsteady linear potential theory. First, general expressions that take into account the effect of any set of unsteady point vortices interacting with the oscillating foil and unsteady wake are derived. Then, a simplified analysis, based on the Brown–Michael model, of the initial stages of the growing LEV from the sharp leading edge during each half-stroke is used to obtain simple expressions for its main contribution to the unsteady lift, thrust and moment. It is found that the LEV contributes to the aerodynamic forces and moment provided that a pitching motion exists, while its effect is negligible, in the present approximation, for a pure heaving motion, and for some combined pitching and heaving motions with large phase shifts which are also characterized in the present work. In particular, the effect of the LEV is found to decrease with the distance of the pivot point from the trailing edge. Further, the time-averaged lift and moment are not modified by the growing LEVs in the present approximation, and only the time-averaged thrust force is corrected, decreasing slightly in most cases in relation to the linear potential results by an amount proportional to $a_0^2 k^3$ for large k, where k is the reduced frequency and a_0 is the pitching amplitude. The time-averaged input power is also modified by the LEV in the present approximation, so that the propulsion efficiency changes by both the thrust and the power, these corrections being relevant only for pivot locations behind the midchord point. Finally, the potential results modified by the LEV are compared with available experimental data.

Key words: aerodynamics, vortex flows

1. Introduction

The leading-edge vortex (LEV) has been proved to be very relevant for the generation of unsteady forces and moment on heaving and pitching airfoils, especially at relatively low Reynolds numbers, being partly responsible for the excellent

† Email address for correspondence: ramon.fernandez@uma.es

aerodynamic performance of flapping wings in insects and small birds (Ellington 1984; Dickinson & Götz 1993; Ellington *et al.* 1996; Wang 2000; Minotti 2002; Wang 2005; Maxworthy 2007; Shyy & Liu 2007; Baik *et al.* 2012; Pitt Ford & Babinsky 2013). However, the unsteady linear potential theory of Theodorsen (1935) and von Kármán and Sears (1938), which assumes small amplitude in the airfoil oscillations, with an almost flat wake vortex sheet and no LEV generation, is surprisingly quite accurate in predicting the unsteady lift force and moment of thin flapping airfoils (McGowan *et al.* 2011; Baik *et al.* 2012; Mackowski & Williamson 2015, 2017; Cordes *et al.* 2017) and also the thrust force and propulsion efficiency when using the correct vortex impulse formulation (Fernandez-Feria 2016, 2017). This is so even for low Reynolds number and for not so small amplitude of the oscillations, when LEV generation and shedding constitutes a relevant feature of the actual fluid motion around the airfoil. Thus, it would be of interest to explore the possibility of including the formation of weak LEVs into the linear potential theory to improve its predictive capabilities when the angle of attack is not very small.

In the present paper, we analyse the interaction of arbitrary travelling point vortices with a heaving and pitching foil within the framework of the unsteady linear potential theory, and obtain general expressions for their contributions to the lift, thrust and moment on the foil by using a vortical impulse formulation (von Kármán & Sears 1938; Wu 1981; Fernandez-Feria 2016). To that end, we solve the integral equation for the vortex-sheet strength of the bound vortex sheet around the foil which takes into account the effect of the point vortices in addition to the free wake vortex sheet. The resulting expressions for the forces and moment contain additional integral terms that depend on the temporal evolution of the point vortices and that, in general, have to be solved numerically.

As a difference from some previous related works, we maintain the continuous trailing vortex wake of the linearized potential theory and add the generation of an LEV during each half-stroke as a point vortex, instead of considering the generation and shedding of both LEVs and trailing-edge vortices (TEVs) as a succession of point vortices. For instance, Tchieu & Leonard (2011) used a vortex theory formulation quite similar to the present one, but considering the trailing wake as a succession of point vortices instead of the continuous distribution of von Kármán & Sears (1938), and without considering the effect of the LEVs, to obtain the lift force and moment of an unsteady thin airfoil. Ramesh *et al.* (2013) extended this approach to large amplitudes, combining the vortex formulation with standard potential theory. Xia & Mohseni (2013) employed conformal mapping and the unsteady Blasius equation to model the force on a pitching flat plate by considering the effect of the LEVs and TEVs as successive point vortices emanating from their respective edges. These authors validated their results against experiments for the starting plate problem and for a non-sinusoidal pitching motion for which our oscillating model is not valid. The starting plate problem, or Wagner problem, was also analysed by Li & Wu (2015) in the presence of additional LEVs/TEVs using a vortical impulse formulation very similar to that developed here. These authors, who only computed the lift force, considered an unsteady developing TEV instead of the long-time infinite trailing vortex wake of an oscillating plate considered here. However, as discussed below in § 3, the general expression for the lift force of a point vortex in terms of the temporal evolution of its circulation and its position, as derived in more detail by Li, Bai & Wu (2015), is equivalent to the general expression developed here. The results for the Wagner problem were generalized by the same authors (Li & Wu 2016) to account for high angles of attack, and for the residual vortex sheet at both the leading and

trailing edges, representing vortices being shed yet not represented by point vortices. A similar general vortex force formulation, without the thin-airfoil assumption, and considering the vortex shedding from a general-shaped airfoil with non-sharp leading edge, was more recently considered by Xia & Mohseni (2017).

To simplify the problem and be able to obtain closed approximate expressions for the forces and moment, we introduce several approximations. First, we assume that the vortices remain sufficiently close to the foil, in accordance with the linearized approximation, and that the thin airfoil has a sharp leading edge, in addition to a sharp trailing edge (as in a flat plate). Then, knowing that the main contribution to the forces and moment is produced while the LEV is still developing close to the leading edge (Pullin & Wang 2004; Martín-Alcántara, Fernandez-Feria & Sanmiguel-Rojas 2015), we consider only the effect of a single developing LEV during each half-stroke, up to the point where it is shed. The last assumption constitutes a strong simplification of the problem, both because all the other already shed LEVs are not taken into account and because the effect of the growing LEV on the wake vorticity is negligible. As a consequence, closed simple expressions for the contribution of the LEV to the forces and moment on the flapping foil can be obtained, constituting a lowest-order correction to the analytical results of the linearized potential theory when the LEV is included in the formulation.

To model the developing LEV, we assume that vorticity is released at the sharp leading edge, with an unsteady Kutta condition to remove the singularity of the bound vortex-sheet strength at the leading edge, similar to the condition applied at the sharp trailing edge where the free wake vortex sheet is released. Then, we use the Brown–Michael model (1954), which ensures momentum conservation (Michelin & Llewellyn Smith 2009) and assumes that the vortex is shed when its circulation reaches an extremum value to avoid discontinuities in temporal forces. More realistic models for the growing and shedding of the vortices could have been used (Tchieu & Leonard 2011; Wang & Eldredge 2013; Hemati, Eldredge & Speyer 2014), but they need additional parameters and equations that would complicate the formulation. The present approximation is in accordance with the simplicity of the linear potential theory, providing closed-form expressions for the contributions of the LEV to the lift, thrust and moment that depend only on flapping kinematics parameters. These results are compared with available experimental data for slender airfoils with small-to-medium maximum angle of attack.

2. Formulation of the problem

We consider the two-dimensional (2D), incompressible and nearly inviscid flow over a heaving and pitching thin airfoil of chord length c that moves with constant speed U along the negative x-axis (see figure 1). The vertical amplitudes of the heaving and pitching motions are both very small compared with c, so that the airfoil and every point of the trail of vortices that it leaves behind may be considered to be on the x-axis in first approximation. In addition to the continuous wake, we shall consider the effect of individual concentrated (point) vortices generated at the leading edge and moving downstream (only one such vortex is depicted in the sketch of figure 1).

For simplicity, we select $c = 2$, so that all lengths are scaled with the half-chord $c/2$, and the plate, or slender airfoil with two sharp ends, extends from $x = -1$ to $x = 1$ in a reference frame translating with it at speed U along the x-axis. In this reference frame, the motion of the airfoil is given by the vertical displacement of its mean-camber line (see the sketch in figure 2),

$$z_s(x, t) = h(t) - (x - a)\alpha(t), \quad -1 \leqslant x \leqslant 1, \tag{2.1}$$

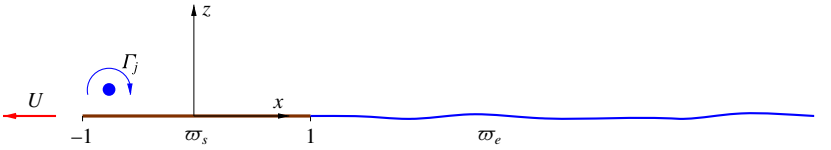

FIGURE 1. (Colour online) Schematic of the problem.

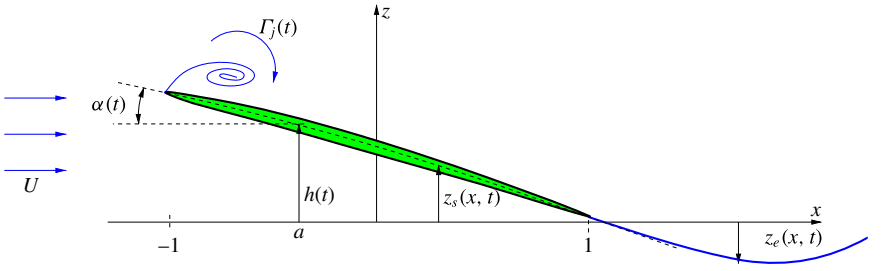

FIGURE 2. (Colour online) Schematic of the oscillating airfoil with an LEV.

with

$$h(t) = \mathrm{Re}[h_0 \mathrm{e}^{\mathrm{i}\omega t}], \quad \alpha(t) = \mathrm{Re}[\alpha_0 \mathrm{e}^{\mathrm{i}\omega t}], \tag{2.2a,b}$$

where ω is the frequency of the oscillations of both the heaving motion, $h(t)$, and the pitching rotation, $\alpha(t)$, around the horizontal axis $x = a$ (i.e. the dimensional pivoting distance from the leading edge is $s_p = (1 + a)c/2$), and Re means real part. The amplitudes h_0 and α_0 are in general complex constants (to account for any phase shift between the two oscillations) satisfying $|h_0| \ll 1$ and $|\alpha_0| \ll 1$. For simplicity, we select h_0 real and

$$\alpha_0 = a_0 \mathrm{e}^{\mathrm{i}\phi}, \tag{2.3}$$

with ϕ the phase shift between the plunging and pitching motions and a_0 the maximum pitching amplitude. In what follows, we shall work with the complex functions, knowing that we have to take the real part of the results. The vertical velocity of the rigid airfoil is

$$v_0(x, t) = \dot{h} - (x - a)\dot{\alpha} - U\alpha, \tag{2.4}$$

where a dot denotes the time derivative.

2.1. *General expressions for the lift, drag or thrust, and moment*

The vortical impulse theory for an incompressible and unbounded flow is used to obtain the forces and moment on the airfoil. Neglecting the volume (section) of the airfoil, one may write (Wu 1981; Saffman 1992; Wu, Ma & Zhou 2006)

$$\boldsymbol{F} \equiv D\boldsymbol{e}_x + L\boldsymbol{e}_z = -\rho \frac{\mathrm{d}\boldsymbol{I}}{\mathrm{d}t}, \tag{2.5}$$

where D is the drag (or minus the thrust) force, L is the lift force, ρ is the fluid density, and the vortical impulse (or vorticity moment) $\boldsymbol{I}$ is defined as

$$\boldsymbol{I} = \int_{\mathcal{V}} \boldsymbol{x} \wedge \boldsymbol{\omega} \, \mathrm{d}\mathcal{V}, \tag{2.6}$$

where $\boldsymbol{\omega} = \boldsymbol{\nabla} \wedge \boldsymbol{v}$ is the vorticity field and $\mathcal{V}$ is the entire volume (plane in this case) occupied by the fluid plus the airfoil. In writing (2.5), it is assumed that $\mathcal{V}$ is unbounded and that the flow is potential far from the airfoil. In fact, we shall assume that the vorticity, which is directed along the normal $\boldsymbol{e}_y$ to the plane of the fluid motion, is concentrated at the airfoil surface, at the trailing wake, both considered as vortex sheets, and at the locations $[x_j(t), z_j(t)]$, $j = 1, \ldots, N$, of the N point vortices (e.g. LEVs) present in the flow at each instant of time. Thus,

$$\boldsymbol{I} \simeq \sum_{j=1}^{N} \Gamma_j(-z_j\boldsymbol{e}_x + x_j\boldsymbol{e}_z) + \int_{-1}^{1} (-z_s\varpi_s\boldsymbol{e}_x + x\varpi_s\boldsymbol{e}_z)\,\mathrm{d}x + \int_{1}^{\infty} (-z_e\varpi_e\boldsymbol{e}_x + x\varpi_e\boldsymbol{e}_z)\,\mathrm{d}x, \quad (2.7)$$

where Γ_j is the circulation (positive clockwise) of the jth point vortex, $\varpi_s(x, t)$, $-1 \leqslant x \leqslant 1$, is the vorticity density distribution on the airfoil, $\varpi_e(x, t)$ is the vorticity density distribution in the trailing wake and $z_e(x, t)$ is the vertical position of each point in this vortex wake. We consider the large-time behaviour in which the vortex wake sheet extends many chord lengths downstream of the airfoil, so that, in first approximation, $1 \leqslant x \leqslant \infty$ for both $\varpi_e(x, t)$ and $z_e(x, t)$, with $|z_e| \ll 1$, as commented on above. Moreover, although the following derivations will be for arbitrary locations of the point vortices (x_j, z_j), we shall simplify them afterwards, retaining only the lowest-order approximations for $|z_j| \ll 1$ to be consistent with the present linearized approach.

Consequently, under the assumptions made, the drag (or minus the thrust) and lift forces on the airfoil are given by

$$D = \rho \sum_{j=1}^{N} \frac{\mathrm{d}}{\mathrm{d}t}(z_j\Gamma_j) + \rho\frac{\mathrm{d}}{\mathrm{d}t}\int_{-1}^{1} z_s\varpi_s\,\mathrm{d}x + \rho\frac{\mathrm{d}}{\mathrm{d}t}\int_{1}^{\infty} z_e\varpi_e\,\mathrm{d}x, \quad (2.8)$$

$$L = -\rho \sum_{j=1}^{N} \frac{\mathrm{d}}{\mathrm{d}t}(x_j\Gamma_j) - \rho\frac{\mathrm{d}}{\mathrm{d}t}\int_{-1}^{1} x\varpi_s\,\mathrm{d}x - \rho\frac{\mathrm{d}}{\mathrm{d}t}\int_{1}^{\infty} x\varpi_e\,\mathrm{d}x. \quad (2.9)$$

Similarly, the vortical impulse theory also provides the moment on the airfoil (Wu 1981; Saffman 1992; Wu *et al.* 2006),

$$\boldsymbol{M} = -M\boldsymbol{e}_y = -\rho\frac{\mathrm{d}\boldsymbol{A}}{\mathrm{d}t}, \quad (2.10)$$

where

$$\boldsymbol{A} = -\frac{1}{2}\int_{\mathcal{V}} |\boldsymbol{x} - a\boldsymbol{e}_x|^2\boldsymbol{\omega}\,\mathrm{d}\mathcal{V} \quad (2.11)$$

is the angular impulse in relation to the pitching axis $x = a$ moving with speed U along the x-axis (it should be noted that the distance Ut is also scaled with $c/2$). Thus,

$$M \simeq \frac{1}{2}\rho\frac{\mathrm{d}}{\mathrm{d}t}\left[\sum_{j=1}^{N}(x_j - Ut + a_i)^2\Gamma_j + \int_{-1}^{1}(x - Ut + a_i)^2\varpi_s\,\mathrm{d}x + \int_{1}^{\infty}(x - Ut + a_i)^2\varpi_e\,\mathrm{d}x\right], \quad (2.12)$$

with $a = Ut - a_i$ in a stationary reference frame with the fluid at rest far from the airfoil.

Without considering the effect of the individual point vortices Γ_j, the lift and moment were computed by von Kármán and Sears (1938) using similar expressions to (2.9) and (2.12), while the thrust/drag was recently computed using (2.8) in Fernandez-Feria (2016). Reference to these works will be made for some particular results needed in the following computations. It should be noted that the general expressions (2.5) and (2.10) were derived by Wu (1981) for any unsteady vorticity distribution in an incompressible flow, including unsteady point vortices. They have already been used for a distribution of unsteady point vortices by Tchieu & Leonard (2011) and Li *et al.* (2015), among others, in similar problems, and (2.5) has also been used for unsteady point vortices to estimate forces from experimental data by Graham, Pitt Ford & Babinsky (2017).

2.2. *Vorticity distribution on the airfoil*

Following von Kármán and Sears (1938) and invoking the linearity of the problem, we separate the contributions of the vortex-sheet wake and the N point vortices to ϖ_s from the bound circulation that would be produced by the motion of the airfoil as if the wake and the point vortices had no effect,

$$\varpi_s(x,t) = \varpi_0(x,t) + \varpi_{1e}(x,t) + \sum_{j=1}^{N} \varpi_{1j}(x,t), \quad -1 \leqslant x \leqslant 1, \tag{2.13}$$

with

$$\Gamma_0(t) = \int_{-1}^{1} \varpi_0(x,t)\,\mathrm{d}x \tag{2.14}$$

being the circulation that would be obtained from the quasisteady airfoil theory, without moving vortices or unsteady wake, such that the corresponding lift would be $\rho U \Gamma_0$. The vorticity density ϖ_{1e} is the contribution to ϖ_s induced by the wake vortex-sheet strength ϖ_e, and ϖ_{1j} is the contribution from the point vortex j. Kelvin's total-circulation conservation theorem requires that

$$\Gamma_0 + \Gamma_{1e} + \sum_{j=1}^{N} (\Gamma_j + \Gamma_{1j}) + \int_1^{\infty} \varpi_e\,\mathrm{d}x = 0, \tag{2.15}$$

with

$$\Gamma_{1e}(t) = \int_{-1}^{1} \varpi_{1e}(x,t)\,\mathrm{d}x \quad \text{and} \quad \Gamma_{1j}(t) = \int_{-1}^{1} \varpi_{1j}(x,t)\,\mathrm{d}x. \tag{2.16a,b}$$

To obtain ϖ_0, ϖ_{1e} and ϖ_{1j}, one has to apply the boundary condition of the vertical velocity (2.4) at $z = 0$, $-1 \leqslant x \leqslant 1$, induced by the whole distribution of vorticity. On separating the three sources, one is led to the following integral equations (e.g. Newman 1977):

$$\frac{1}{2\pi} \fint_{-1}^{1} \frac{\varpi_0(\xi,t)}{\xi - x}\,\mathrm{d}\xi = v_0(x,t), \tag{2.17}$$

$$\frac{1}{2\pi} \fint_{-1}^{1} \frac{\varpi_{1e}(\xi,t)}{\xi - x}\,\mathrm{d}\xi = -\frac{1}{2\pi} \int_1^{\infty} \frac{\varpi_e(\xi,t)}{\xi - x}\,\mathrm{d}\xi, \tag{2.18}$$

$$\frac{1}{2\pi}\fint_{-1}^{1}\frac{\varpi_{1j}(\xi,t)}{\xi-x}\,\mathrm{d}\xi=\frac{\Gamma_j}{2\pi}\frac{x-x_j}{(x-x_j)^2+z_j^2},\quad j=1,\ldots,N, \tag{2.19}$$

where $\fint$ denotes Cauchy's principal value of the integral. The contribution from the unsteady planar wake, ϖ_e, was derived by von Kármán and Sears (1938) using the circle plane from Joukowski conformal mapping, instead of solving (2.18), to obtain, after applying the Kutta condition at the trailing edge, $x=1$,

$$\varpi_{1e}(x,t)=\frac{1}{\pi}\int_1^\infty\sqrt{\frac{\xi+1}{\xi-1}}\sqrt{\frac{1-x}{1+x}}\frac{\varpi_e(\xi,t)}{(\xi-x)}\,\mathrm{d}\xi, \tag{2.20}$$

which, integrated between $x=-1$ and $x=1$, yields

$$\Gamma_{1e}(t)=\int_1^\infty\left(\sqrt{\frac{\xi+1}{\xi-1}}-1\right)\varpi_e(\xi,t)\,\mathrm{d}\xi. \tag{2.21}$$

The solutions to (2.17) and (2.19) satisfying (2.14) and (2.16*a*,*b*) can be formally written as (e.g. Newman 1977; Carrier, Krook & Pearson 2005)

$$\varpi_0(x,t)=\frac{2}{\pi\sqrt{1-x^2}}\left[\frac{\Gamma_0(t)}{2}-\fint_{-1}^{1}\frac{\sqrt{1-\xi^2}}{\xi-x}v_0(\xi,t)\,\mathrm{d}\xi\right], \tag{2.22}$$

$$\varpi_{1j}(x,t)=\frac{2}{\pi\sqrt{1-x^2}}\left[\frac{\Gamma_{1j}(t)}{2}-\frac{\Gamma_j(t)}{2\pi}\fint_{-1}^{1}\frac{\sqrt{1-\xi^2}}{\xi-x}\frac{\xi-x_j(t)}{[\xi-x_j(t)]^2+z_j(t)^2}\,\mathrm{d}\xi\right]. \tag{2.23}$$

On the other hand, the Kutta condition at the trailing edge, i.e. the regularity of ϖ_s at the trailing edge, implies that the terms in brackets vanish, so that

$$\Gamma_0(t)=-2\fint_{-1}^{1}\sqrt{\frac{1+\xi}{1-\xi}}v_0(\xi,t)\,\mathrm{d}\xi=2\pi\left[U\alpha-\dot{h}-\left(a-\frac{1}{2}\right)\dot{\alpha}\right], \tag{2.24}$$

$$\Gamma_{1j}(t)=C_j(t)\Gamma_j(t),\quad\text{with } C_j(t)\equiv-\frac{1}{\pi}\fint_{-1}^{1}\sqrt{\frac{1+\xi}{1-\xi}}\frac{\xi-x_j(t)}{[\xi-x_j(t)]^2+z_j(t)^2}\,\mathrm{d}\xi. \tag{2.25}$$

On substituting (2.21) and (2.25) into (2.15), the following relation between Γ_0, Γ_j and ϖ_e is obtained:

$$\Gamma_0(t)+\sum_{j=1}^{N}\Gamma_j(t)[1+C_j(t)]+\int_1^\infty\sqrt{\frac{\xi+1}{\xi-1}}\varpi_e(\xi,t)\,\mathrm{d}\xi=0. \tag{2.26}$$

The general expression for the vorticity distribution on the airfoil is obtained by substituting (2.20), (2.22) and (2.23), together with (2.24) and (2.25), into (2.13),

$$\varpi_s(x,t)=\frac{1}{\pi}\sqrt{\frac{1-x}{1+x}}\left\{-\fint_{-1}^{1}\left[2v_0(\xi,t)+\sum_{j=1}^{N}\frac{\Gamma_j(t)}{\pi}\frac{\xi-x_j(t)}{(\xi-x_j(t))^2+z_j^2(t)}\right]\sqrt{\frac{1+\xi}{1-\xi}}\frac{\mathrm{d}\xi}{\xi-x}\right.$$
$$\left.+\int_1^\infty\sqrt{\frac{1+\xi}{\xi-1}}\frac{\varpi_e(\xi,t)}{\xi-x}\,\mathrm{d}\xi\right\}. \tag{2.27}$$

It should be noted that this bound vortex-sheet strength is singular at the leading edge, $x=-1$. However, we will apply in § 4.1 below the Kutta condition at the leading edge while an LEV (Γ_1, say) is developing, so that ϖ_s will also be regular at $x=-1$ during the fraction of the half-stroke when the LEV is growing from the leading edge.

Kelvin's theorem (2.26) provides an integral equation for the trailing-edge vortex-sheet strength ϖ_e in terms of the quasisteady circulation $\Gamma_0(t)$, given by (2.22) as a function of the foil motion $v_0(x,t)$, and the circulation $\Gamma_j(t)$ and trajectory $[x_j(t), z_j(t)]$ of each point vortex present in the flow, which have to be modelled independently (see § 4 below). Thus, (2.26)–(2.27) suffice to obtain general expressions for the lift, thrust and moment on the foil in terms of $v_0(x,t)$, $\Gamma_j(t)$ and $[x_j(t), z_j(t)]$, $j=1,\ldots,N$, which are derived next. A comment on the above particular application of the Kutta condition at the trailing edge and the general validity of (2.26)–(2.27) is given in appendix A.

3. Force and moment for arbitrary movements of the point vortices and foil

Before simplifying the above expressions for the oscillatory motion (2.1)–(2.2) of the airfoil and before implementing models for the generation and evolution of the LEVs in each stroke of the airfoil, it is instructive to write the general expressions for the forces and moment within the present linearized approximation.

To compute the temporal derivatives of terms containing ϖ_e and z_e, one assumes that the vorticity in the wake is convected downstream with velocity U, so that both remain constant in a reference frame moving with the fluid (von Kármán & Sears 1938; Newman 1977),

$$\varpi_e(\xi,t)=\varpi_e(X), \quad z_e(\xi,t)=z_e(X), \quad \text{with } X=\xi-Ut. \tag{3.1a,b}$$

Consequently, the time derivatives of the terms containing the wake vorticity ϖ_e may be easily computed using Leibniz's rule. Taking also into account the circulation conservation (2.26) and the integrals given in appendix B, one obtains the following expression for the lift (2.9):

$$L=L_0+L_1+L_2+\sum_{j=1}^{N}L_{lj}, \tag{3.2}$$

where

$$L_0=\rho U\Gamma_0, \quad L_1=\pi\rho(U\dot{\alpha}-\ddot{h}-a\ddot{\alpha}), \quad L_2=\rho U\int_1^\infty \frac{\varpi_e}{\sqrt{\xi^2-1}}\,\mathrm{d}\xi \tag{3.3a–c}$$

are the quasisteady lift, the apparent mass lift and the unsteady wake lift respectively obtained by von Kármán & Sears (1938), and the contribution from each jth point vortex is

$$L_{lj}=\rho\left\{U\Gamma_j(1+C_j)-\frac{\mathrm{d}}{\mathrm{d}t}[\Gamma_j(x_j+D_j)]\right\}, \tag{3.4}$$

with D_j defined in (B 3) in appendix B. This last expression coincides with that derived by Li *et al.* (2015) for point vortices when D_j is interpreted as the x coordinate of the image of the vortex j inside the foil. With this proviso, although obtained from a quite different approach, it also agrees with the results of Xia & Mohseni (2013) under the constant circulation assumption, with the vortices

contributing to the force through vortex convection (including the image vortices) and vortex variation. The first term of (3.4) is basically the Kutta–Joukowski theorem applied to the circulation Γ_j of the individual vortex itself plus its induced circulation $\Gamma_{1j} = \Gamma_j C_j$ around the foil. The second term is the unsteady contribution to the lift force due to the motion of the vortex and its variation in intensity, including the induced vorticity on the foil. It says that positive lift on the airfoil is generated if $\Gamma_j x_j$ decreases in time, as happens, for instance, at the initial stages of the formation of the LEV at the beginning of each downstroke, when the LEV starts to move upstream of the leading edge ($x_j \leqslant -1$, see § 4.1 below for the details) with its circulation Γ_j growing in time. The opposite happens in the initial stages of the formation of the LEV during the beginning of the upstroke, where $\Gamma_j < 0$ and decreases (it should be remembered that we use $\Gamma > 0$ for a clockwise vortex), moving also upstream of the leading edge. When Γ_j is constant, the expression coincides with the well-known vortex force produced by a free vortex (Saffman 1992; Alaminos-Quesada & Fernandez-Feria 2017). If the free vortex (Γ_j independent of time) is far away from the foil ($x_j^2 + z_j^2 \to \infty$), and therefore moving with the free stream velocity, $\mathrm{d}x_j/\mathrm{d}t = U$, one has that $L_{lj} \to 0$ since both C_j and D_j tend to zero with the distance from the foil. Incidentally, this is the reason why we can disregard the effect on the lift force of the starting vortex at infinity in the present impulse formulation.

The lift expression (3.2) can be rewritten in a more convenient form by grouping together L_0 and the first term in L_{li} after using the total circulation conservation (2.26),

$$L = L_a + L_e + \sum_{j=1}^{N} L_j, \tag{3.5}$$

where $L_a \equiv L_1$ is the added mass term given in (3.3) and the net contributions from the wake and each point vortex j are respectively

$$L_e = -\rho U \int_1^\infty \frac{\xi \varpi_e}{\sqrt{\xi^2 - 1}}\,\mathrm{d}\xi, \tag{3.6}$$

$$L_j = -\rho \frac{\mathrm{d}}{\mathrm{d}t}[\Gamma_j (x_j + D_j)]. \tag{3.7}$$

It should be noted, however, that the effect of the point vortices on the wake vorticity distribution ϖ_e has to be obtained from (2.26).

Similarly, by using some of the integrals given in appendix B, the drag (2.8) can be written as

$$\begin{aligned} D \;=\; & \rho \sum_{j=1}^{N} \frac{\mathrm{d}}{\mathrm{d}t}\{\Gamma_j[z_j + (h + a\alpha)C_j - \alpha D_j]\} + \rho \frac{\mathrm{d}}{\mathrm{d}t}[(h + a\alpha)\Gamma_0] - \pi\rho \frac{\mathrm{d}}{\mathrm{d}t}[\alpha(\dot{h} + a\dot{\alpha} - U\alpha)] \\ & + \rho \frac{\mathrm{d}}{\mathrm{d}t} \int_1^\infty \varpi_e \left[\left(\sqrt{\frac{\xi + 1}{\xi - 1}} - 1 \right)(h + a\alpha) - (\sqrt{\xi^2 - 1} - \xi)\alpha + z_e \right] \mathrm{d}\xi. \end{aligned} \tag{3.8}$$

For the vertical displacement of the wake z_e, we assume that it coincides with the trailing-edge location at the time $t' = t + (1 - \xi)/U$ when it was shed from the airfoil, $z_s(x = 1, t')$, i.e.

$$z_e(X) = h\left(\frac{1 - X}{U}\right) - (1 - a)\alpha\left(\frac{1 - X}{U}\right). \tag{3.9}$$

Thus,

$$\frac{\mathrm{d}}{\mathrm{d}t}\int_1^\infty z_e\varpi_e\,\mathrm{d}\xi = U[h(t)-(1-a)\alpha(t)]\varpi_e(\xi=1,t). \tag{3.10}$$

Using also (2.26) and (3.3)–(3.4), the thrust $T=-D$ from (3.8) can be written as

$$T=-\alpha L+T_1+T_2+\sum_{j=1}^{N}T_{lj}, \tag{3.11}$$

where

$$T_1=\pi\rho\dot{\alpha}(\dot{h}+a\dot{\alpha}-\alpha U),\quad T_2=\rho\int_1^\infty[\dot{h}+\dot{\alpha}(\sqrt{\xi^2-1}-\xi+a)-\alpha U]\varpi_e\,\mathrm{d}\xi, \tag{3.12a,b}$$

$$T_{lj}=\rho\frac{\mathrm{d}}{\mathrm{d}t}[\Gamma_j(h+a\alpha-z_j-\alpha x_j)]+\rho\dot{\alpha}\Gamma_j(x_j+D_j). \tag{3.13}$$

The first term in (3.11) is the component in the flight direction of the force normal to the airfoil, with L given by (3.2). The second and third terms are the contributions to the thrust from the apparent mass and the vorticity distribution in the wake respectively, already obtained in Fernandez-Feria (2016), while the fourth term is the contribution from the point vortices. It should be noted that the length in the first term of (3.13), $h+a\alpha-z_j-\alpha x_j$, is minus the vertical position of the point vortex in relation to the plate, $z_s(x_j)-z_j$, if $-1\leqslant x_j\leqslant 1$.

Part of the contribution from the vortex j is actually included in the first term of (3.11) (inside L). Thus, it is convenient to use (3.5) and rewrite the thrust in a similar fashion to the lift (3.5),

$$T=T_a+T_e+\sum_{j=1}^{N}T_j, \tag{3.14}$$

where

$$T_a=-\alpha L_a+T_1=\pi\rho\frac{\mathrm{d}}{\mathrm{d}t}[\alpha(\dot{h}+a\dot{\alpha}-\alpha U)] \tag{3.15}$$

is the added mass thrust,

$$T_e=-\alpha L_e+T_2=\rho\int_1^\infty\left[\dot{h}+\dot{\alpha}(\sqrt{\xi^2-1}-\xi+a)-\alpha U\left(1+\frac{\xi}{\sqrt{\xi^2-1}}\right)\right]\varpi_e\,\mathrm{d}\xi \tag{3.16}$$

is the contribution from the unsteady wake and

$$T_j=\rho\frac{\mathrm{d}}{\mathrm{d}t}\{\Gamma_j[z_s(x_j)-z_j+\alpha(x_j+D_j)]\} \tag{3.17}$$

is the contribution from the point vortex j (it should be noted that there is an additional contribution of the point vortices in ϖ_e through the total circulation conservation (2.26)). For a free vortex (Γ_j constant), T_j is proportional to minus the temporal variation of the vertical distance of the vortex from the plate, plus a similar contribution coming from the induced vorticity on the plate, whose vertical distance is represented by $-\alpha D_j$. In general, this term T_j contributes to positive thrust when $-\Gamma_j z_j$ increases, so that the formation of the LEV generates negative thrust at the initial stages of both the downstroke and the upstroke (see § 5 below for more details).

Finally, using the above expressions and some integrals from appendix B, the moment (2.12) can be written as

$$M = M_a + M_e + \sum_{j=1}^{N} M_j, \tag{3.18}$$

where

$$M_a = -\rho \frac{\mathrm{d}}{\mathrm{d}t}\left[\frac{a}{2}(\pi\dot{\alpha} - \Gamma_0) + \frac{\pi\dot{\alpha}}{8}\right] \tag{3.19}$$

is the contribution from the added mass,

$$M_e = \frac{1}{2}\rho U \int_1^\infty \frac{1 - 2a\xi}{\sqrt{\xi^2 - 1}} \varpi_e \,\mathrm{d}\xi \tag{3.20}$$

is the contribution from the unsteady wake and

$$M_j = \rho \frac{\mathrm{d}}{\mathrm{d}t}\left\{\Gamma_j\left[\frac{x_j^2}{2} + \frac{E_j}{2} - \frac{1}{4} - a(x_j + D_j)\right]\right\} \tag{3.21}$$

is the contribution from the point vortex j, with E_j defined in (B 4) in appendix B.

4. Evolution of the point vortices, including the developing LEV

4.1. *General model*

In the above general expressions, the contribution of each point vortex j to the lift, thrust and moment on the airfoil depends on time through the vortex intensity $\Gamma_j(t)$ and its trajectory $[x_j(t),\, z_j(t)]$. Part of this dependence is inside the integrals $C_j[x_j(t),\, z_j(t)]$, $D_j[x_j(t),\, z_j(t)]$ and $E_j[x_j(t),\, z_j(t)]$ defined in (2.25), (B 3) and (B 4) respectively. In addition, the wake vorticity ϖ_e is also affected by the evolution of this point vortex j through Kelvin's theorem (2.26). Therefore, one needs three additional equations for each point vortex to obtain $\Gamma_j(t)$, $x_j(t)$ and $z_j(t)$, which have to be solved together with the integral equation (2.26) for $\varpi_e(x, t)$, with $\Gamma_0(t)$ given by (2.24), once the vertical movement of the airfoil $v_0(x, t)$ is prescribed.

As a first simplification to the problem, it is assumed that, during each half-stroke, there is only one developing LEV, labelled by $j = 1$. The remaining vortices, $j = 2, \ldots, N$, have already been shed, so that they move with the Kirchhoff velocity and their intensities are frozen (Tchieu & Leonard 2011; Wang & Eldredge 2013),

$$\frac{\mathrm{d}\Gamma_j}{\mathrm{d}t} = 0\,, \quad \frac{\mathrm{d}x_j}{\mathrm{d}t} - \mathrm{i}\frac{\mathrm{d}z_j}{\mathrm{d}t} = \mathrm{v}^*[\mathrm{z}_j(t)], \quad j = 2, 3, \ldots, \tag{4.1}$$

where $\mathsf{z}_j = x_j + \mathrm{i}z_j$ is the position of the point vortex j on the complex plane and

$$\mathsf{v}^*[\mathsf{z}_j(t)] \equiv \bar{u}_j - \mathrm{i}\bar{v}_j = U - \frac{\mathrm{i}}{2\pi}\int_{-1}^{1} \varpi_s(x,t)\frac{\mathrm{d}x}{x-\mathsf{z}_j} - \frac{\mathrm{i}}{2\pi}\int_{1}^{\infty} \varpi_e(x,t)\frac{\mathrm{d}x}{x-\mathsf{z}_j} + \sum_{k\neq j}\frac{\mathrm{i}\Gamma_k}{2\pi(\mathsf{z}_j-\mathsf{z}_k)} \tag{4.2}$$

is the complex conjugate velocity at the vortex centre z_j excluding the self-contribution of the vortex. The initial conditions for these differential equations are the values of Γ_j, x_j and z_j at the shedding instant t_{js}, $j = 2, 3, \ldots$.

Since Γ_1 is developing from the sharp leading edge, one has to apply the Kutta condition at $x = -1$ to remove the singularity of ϖ_s given by (2.27). It should be noted that this condition has already been applied at the trailing edge, where the unsteady wake is continuously generated, in the derivation of ϖ_0, ϖ_{1j} and ϖ_{1e}, so that ϖ_s given by (2.27) is not singular at $x = 1$. Thus, (2.27) has to be regular also at the leading edge while $|\Gamma_1|$ is growing, which means that the term inside brackets has to vanish at $x = -1$,

$$\fint_{-1}^{1}\left[2v_0(\xi,t) + \sum_{j=1}^{N}\frac{\Gamma_j(t)}{\pi}\frac{\xi - x_j(t)}{(\xi-x_j(t))^2 + z_j^2(t)}\right]\frac{\mathrm{d}\xi}{\sqrt{1-\xi^2}} = \int_{1}^{\infty}\frac{\varpi_e(\xi,t)}{\sqrt{\xi^2-1}}\,\mathrm{d}\xi. \tag{4.3}$$

This additional relation is similar to (2.26) and can be written as

$$\Gamma_0 - \pi\dot{\alpha} + \sum_{j=1}^{N}\Gamma_j B_j + \int_{1}^{\infty}\frac{\varpi_e(\xi,t)}{\sqrt{\xi^2-1}}\,\mathrm{d}\xi = 0, \tag{4.4}$$

where

$$B_j \equiv -\frac{1}{\pi}\fint_{-1}^{1}\frac{\xi - x_j}{(\xi-x_j)^2 + z_j^2}\frac{\mathrm{d}\xi}{\sqrt{1-\xi^2}}. \tag{4.5}$$

With this new condition, the vorticity distribution (2.27) is now also regular at the leading edge, $x = -1$, and can be written as

$$\varpi_s(x,t) = \frac{1}{\pi}\sqrt{1-x^2}\left[2\pi\dot{\alpha} - \sum_{j=1}^{N}\frac{\Gamma_j(t)}{\pi}\fint_{-1}^{1}\frac{\xi - x_j(t)}{(\xi-x_j(t))^2 + z_j^2(t)}\frac{\mathrm{d}\xi}{\sqrt{1-\xi^2}(\xi-x)} + \int_{1}^{\infty}\frac{\varpi_e(\xi,t)}{\sqrt{\xi^2-1}(\xi-x)}\,\mathrm{d}\xi\right]. \tag{4.6}$$

As the two additional conditions for Γ_1, x_1 and z_1 we shall use the Brown–Michael (1954) equation, which ensures the momentum conservation around the vortex and the branch cut between the point vortex and the leading edge (Michelin & Llewellyn Smith 2009),

$$\frac{\mathrm{d}\mathsf{z}_1}{\mathrm{d}t} + \frac{\mathsf{z}_1 - \mathsf{z}_{10}}{\Gamma_1}\frac{\mathrm{d}\Gamma_1}{\mathrm{d}t} = \mathsf{v}(\mathsf{z}_1), \tag{4.7}$$

where $\mathsf{v}(\mathsf{z}_1) = \bar{u}_1 + \mathrm{i}\bar{v}_1$ is given by (4.2) for $\mathsf{z}_1 = x_1 + \mathrm{i}z_1$. These are two differential equations which have to be solved with the initial condition at the beginning of each half-stroke, $t = t_i$,

$$\Gamma_1(t_i) = 0, \quad x_1(t_i) = x_{10} = -1, \quad z_1(t_i) = z_{10}(t_i) = z_s(-1, t_i), \tag{4.8a–c}$$

where t_i is given by

$$\left.\frac{\mathrm{d}z_s}{\mathrm{d}t}\right|_{x=-1, t=t_i} = \dot{h}(t_i) + (1+a)\dot{\alpha}(t_i) = 0. \tag{4.9}$$

The point vortex with growing circulation $\Gamma_1(t)$ is shed when Γ_1 reaches an extremum value, $\mathrm{d}\Gamma_1/\mathrm{d}t = 0$. After that, the circulation remains constant and, according to (4.7), the vortex travels with the Kirchhoff velocity. This shedding criterion is that when the strength of a vortex reaches an extremum, it is frozen at that value and the vortex subsequently moves according to the Kirchhoff velocity, avoids a discontinuity in the temporal variation of the impulse, and therefore in the force. One could have used, instead of the Brown–Michael equation (4.7), the impulse matching model of Wang and Eldredge (2013), which avoids this discontinuity even when the vortex is shed without reaching an extremum intensity. However, it would need an additional, experimentally or numerically based, shedding condition which would have complicated the formulation.

On the other hand, any vortex-shedding model based on just three parameters, like the present one, namely the circulation Γ_1 of a point vortex moving with trajectory $[x_1(t), z_1(t)]$ from the leading edge, cannot satisfy at the same time the Kutta condition at the sharp edge, and the conservation around the vortex and branch cut between the leading edge and the vortex of the linear momentum in both directions and the angular momentum. The Brown–Michael (1954) model satisfies the conservation of linear momentum (Michelin & Llewellyn Smith 2009), avoiding a spurious net force on the foil, but introducing a spurious torque (Brown & Michael 1954; Howe 1996; Michelin & Llewellyn Smith 2009; Tchieu & Leonard 2011). Howe (1996) developed an alternative approach satisfying the conservation of angular momentum, more appropriate to determine sound generation. We think that the Brown–Michael model is more appropriate here where the main aim is to determine the forces on the foil.

4.2. *Simplified model. Non-dimensional variables*

To simplify the problem, we shall only consider the effect of the growing LEV with circulation $\Gamma_1(t)$ at each half-stroke, disregarding the effect of the remaining, already shed, vortices. In addition, to simplify the notation, we shall only use, from this point on, non-dimensional variables. All lengths are already scaled with the semichord $c/2$. The remaining non-dimensional variables are (the same letter is used in most of them for the sake of simplicity)

$$t \leftarrow \frac{2tU}{c}, \quad \bar{u}_1, \bar{v}_1 \leftarrow \frac{\bar{u}_1}{U}, \frac{\bar{v}_1}{U}, \quad \Gamma_1 \leftarrow \frac{\Gamma_1}{Uc/2}, \quad \text{etc.} \tag{4.10a–c}$$

From (4.9) and (2.2)–(2.3), the non-dimensional initial time t_i at the beginning of each half-stroke is given by

$$kt_i = \arctan\left[-\frac{(1+a)a_0 \sin\phi}{h_0 + (1+a)a_0\cos\phi}\right] \pm n\pi, \quad n = 0, 1, 2, \ldots, \tag{4.11}$$

where

$$k = \frac{c\omega}{2U} \tag{4.12}$$

is the reduced frequency (it should be noted that kt_i with t_i non-dimensional is equal to ωt_i with t_i dimensional). For a pure heaving motion, $kt_i = \pm n\pi$, while for a pure pitching motion, $kt_i = -\phi \pm n\pi$, but we may set $\phi = 0$ since there is no combined motion. It should be noted that the non-dimensional half-period is π/k.

For each half-stroke, we reset the non-dimensional time by using

$$\tau = t - t_i \tag{4.13}$$

and define

$$\theta(\tau) = x_{10} - x_1 = -1 - x_1(t), \quad \zeta(\tau) = z_1(t) - z_{10}(t) = z_1(t) - [h(t) + (1+a)\alpha(t)], \tag{4.14a,b}$$

with initial conditions

$$\theta(0) = \zeta(0) = 0. \tag{4.15}$$

For the initial stages of the developing LEV, it is assumed that

$$0 \leqslant \theta \ll 1, \quad |\zeta| \ll 1, \tag{4.16a,b}$$

the last condition being implied by the present linearized formulation, where $|z_1| \ll 1$. In fact, we shall use below z_1, and then substitute it by ζ according to (4.14).

From (2.25), neglecting terms of order z_1^2, one obtains

$$C_1 \simeq -1 + \sqrt{\frac{x_1+1}{x_1-1}} \simeq -1 + \sqrt{\frac{\theta}{2}}. \tag{4.17}$$

Consequently, from Kelvin's circulation theorem (2.26), the growing LEV has a negligible effect on the wake vorticity ϖ_e when $\theta \ll 1$, so that ϖ_e depends, in first approximation, only on Γ_0,

$$\int_1^\infty \sqrt{\frac{\xi+1}{\xi-1}}\varpi_e(\xi, t)\,\mathrm{d}\xi \simeq -\Gamma_0(t). \tag{4.18}$$

From (2.24), and for the oscillatory motion (2.2)–(2.3), Γ_0 can be written in non-dimensional form as

$$\Gamma_0(t) = G_0 \mathrm{e}^{\mathrm{i}kt}, \quad G_0 = 2\pi[\alpha_0 - \mathrm{i}kh_0 - \mathrm{i}k(a-1/2)\alpha_0]. \tag{4.19a,b}$$

Thus, (A 2) has the well-known solution (Theodorsen 1935; von Kármán & Sears 1938)

$$\varpi_e(\xi, t) = g\mathrm{e}^{\mathrm{i}k(t-\xi)}, \tag{4.20}$$

$$g = -\frac{G_0}{\displaystyle\int_1^\infty \sqrt{\frac{\xi+1}{\xi-1}}\mathrm{e}^{-\mathrm{i}k\xi}\,\mathrm{d}\xi} = \frac{2G_0}{\pi}\frac{1}{\mathrm{i}H_0^{(2)}(k) + H_1^{(2)}(k)}, \tag{4.21}$$

where $H_n^{(2)}(z) = J_n(z) - \mathrm{i}Y_n(z)$, $n = 0, 1$, are Hankel functions, related to the Bessel functions J_n and Y_n (see, e.g., Olver & Maximon 2010).

From the Kutta condition (4.4) at the leading edge, one can obtain Γ_1 as a function of the position of the vortex and the parameters of the problem. To that end, one has first to compute the integral (4.5) defining B_1 and the integral involving ϖ_e in (4.4). Neglecting terms of $O(z_1)^2$, B_1 is given by

$$B_1 \simeq -\frac{1}{\sqrt{2\theta}}, \tag{4.22}$$

while

$$\int_1^\infty \frac{\varpi_e(\xi, t)}{\sqrt{\xi^2-1}}\,\mathrm{d}\xi = -\mathrm{i}\Gamma_0 \frac{H_0^{(2)}(k)}{\mathrm{i}H_0^{(2)}(k)+H_1^{(2)}(k)}, \tag{4.23}$$

which, after substituting in (4.4), yields

$$\Gamma_1(t) \simeq \sqrt{2\theta(t)}[\Gamma_0(t)C(k) - \pi\dot{\alpha}] = \sqrt{2\theta(t)}\mathcal{G}(t), \tag{4.24}$$

where

$$\mathcal{G} \equiv \Gamma_0 C - \pi\dot{\alpha} = 2\pi[\alpha - \dot{h} - (a-\tfrac{1}{2})\dot{\alpha}]C(k) - \pi\dot{\alpha} \tag{4.25}$$

and

$$C(k) \equiv \frac{H_1^{(2)}(k)}{\mathrm{i}H_0^{(2)}(k)+H_1^{(2)}(k)} \equiv F(k) + \mathrm{i}G(k) \tag{4.26}$$

is the Theodorsen function (Theodorsen 1935; Garrick 1938). (It is understood that one has to take the real parts of all of the complex quantities separately.) This expression for Γ_1 says that, at the initial stages, the LEV approximately grows as the square root of the distance from the leading edge θ, but modulated by the oscillatory motion of the airfoil through $\mathcal{G}(t)$.

To write the equations for $x_1(t)$ and $z_1(t)$ (or $\zeta(t)$) from the Brown–Michael equation (4.7), we need the Kirchhoff velocity components $\bar{u}_1$ and $\bar{v}_1$, which are obtained from the non-dimensional form of (4.2). Since the single LEV is very close to the leading edge, we shall only consider the effect of the vorticity distribution (4.6) on the foil generated by the foil movement, i.e. $\varpi_s(x,t) \approx \varpi_0(x,s) = 2\dot{\alpha}\sqrt{1-x^2}$. Thus,

$$\mathrm{v}^*[\mathrm{z}_1(t)] \equiv \bar{u}_1 - \mathrm{i}\bar{v}_1 \simeq 1 - \frac{\mathrm{i}\dot{\alpha}}{\pi}\int_{-1}^{1}\frac{\sqrt{1-x^2}}{x-\mathrm{z}_1} = 1 + \mathrm{i}\dot{\alpha}\mathrm{z}_1\left(1-\sqrt{1-\frac{1}{\mathrm{z}_1^2}}\right). \tag{4.27}$$

To be consistent with the present linearized theory, one may neglect terms of order z_1^2 to write

$$\bar{u}_1 - \mathrm{i}\bar{v}_1 \simeq 1 + \frac{z_1\dot{\alpha}}{\sqrt{x_1^2-1}}\left(\frac{x_1^2}{|x_1|} - \sqrt{x_1^2-1}\right) + \mathrm{i}\dot{\alpha}\left(x_1 - \frac{x_1}{|x_1|}\sqrt{x_1^2-1}\right). \tag{4.28}$$

On substituting these expressions for $\bar{u}_1$ and $\bar{v}_1$, together with (4.24) and (4.14), into the Brown–Michael equation (4.7), two differential equations for $\theta(\tau)$ and $\zeta(\tau)$ result,

$$\frac{\mathrm{d}}{\mathrm{d}\tau}(\theta^{3/2}\mathcal{G}) = -\mathcal{G}\theta^{1/2}\bar{u}_1, \quad \frac{\mathrm{d}}{\mathrm{d}\tau}(\zeta\theta^{1/2}\mathcal{G}) = \mathcal{G}\theta^{1/2}\left(\bar{v}_1 - \frac{\mathrm{d}z_{10}}{\mathrm{d}\tau}\right), \tag{4.29}$$

which have to be solved numerically with the initial conditions (4.15). For small θ, (4.28) can be approximated by

$$\bar{u}_1 \simeq 1 + \frac{z_1\dot{\alpha}}{\sqrt{2\theta}}\left(1 - \sqrt{2\theta} + \frac{3}{4}\theta\right), \quad \bar{v}_1 \simeq \dot{\alpha}(1 - \sqrt{2\theta} + \theta). \tag{4.30a,b}$$

Since $\tau = 0$ is a singular point of the equations, the numerical integration has to be started from an analytical approximation for $\tau \ll 1$. Retaining only the leading terms in (4.30) for $\theta \ll 1$ and $\zeta \ll 1$ (see (4.14)), the lowest order of (4.29) can be written as

$$\frac{\mathrm{d}}{\mathrm{d}\tau}(\theta^{3/2}\mathcal{G}) \simeq -\frac{\mathcal{G}z_{10}\dot{\alpha}}{\sqrt{2}}, \quad \frac{\mathrm{d}}{\mathrm{d}\tau}(\zeta\theta^{1/2}\mathcal{G}) \simeq \theta^{1/2}\mathcal{G}(\dot{\alpha} - \dot{z}_{10}), \tag{4.31a,b}$$

which have to be solved with the initial conditions (4.15). These equations can be formally integrated to yield

$$\theta \simeq \left(-\frac{1}{\sqrt{2}\mathcal{G}}\int_0^\tau \mathcal{G}z_{10}\dot{\alpha}\,\mathrm{d}\tau\right)^{2/3}, \quad \zeta \simeq \frac{1}{\theta^{1/2}\mathcal{G}}\int_0^\tau \theta^{1/2}\mathcal{G}(\dot{\alpha} - \dot{z}_{10})\,\mathrm{d}\tau. \tag{4.32a,b}$$

The initial approximation to start the numerical integration of (4.29) can be obtained by approximating the above analytical solution for $\tau = t - t_i \ll 1$ using the expansions of $z_{10}(\tau)$, $\alpha(\tau)$ and $\mathcal{G}(\tau)$ for $\tau \ll 1$ given in appendix C. On substituting these expansions into (4.32), at the lowest order for $\tau \ll 1$, one obtains

$$\theta \simeq \left(-\frac{z_{100}\alpha_{i1}}{\sqrt{2}}\right)^{2/3}\tau^{2/3} = \left(\frac{kh_0a_0\sin\phi}{\sqrt{2}}\right)^{2/3}\tau^{2/3}, \quad \zeta \simeq \frac{3\alpha_{i1}}{4}\tau, \tag{4.33a,b}$$

where z_{100} and α_{i1} are given in appendix C. The time dependences in these expressions, and the corresponding $\Gamma_1 \propto \tau^{1/3}$ after substituting into (4.24), coincide with those at the leading order of the solution for the growth of a vortex sheet from the leading edge of a starting flat plate when considered as a point vortex (Pullin & Wang 2004). These expressions are not valid, and therefore cannot be used to start the numerical integration, if h_0, a_0 or $\sin\phi$ vanishes. These particular cases will be considered separately below.

Figures 3 and 4 show some results for $h_0 = 0.1$, $a_0 = 20°$, $a = 0$ and $k = 5$, with $\phi = 10°$ and $\phi = 90°$ respectively. In figures 3(*a*) and 4(*a*), we plot the trajectories $\zeta(\tau)$ versus $x_1(\tau)$ (it should be noted that the initial value of x_1 is -1, and $z_1(\tau) = z_{10}(\tau) + \zeta(\tau)$). We integrate (4.29)–(4.30) numerically starting from a sufficiently small value of τ with (4.33) until $\Gamma_1(\tau)$, plotted in figures 3(*b*) and 4(*b*), reaches a maximum value, marked with circles in the vortex trajectories. From this point on, the circulation Γ_1 remains constant and we integrate (4.7) without the second term. For the numerical integrations, we use the general expression (4.28) for $\bar{u}_1$ and $\bar{v}_1$, valid for any x_1, and the solver `ode15s` from MATLAB. Since most of the vortex contribution to the forces and moment occurs, as we shall see, before the vortex is shed, and this event happens in both plotted cases before the vortex passes above (below) the foil, we only plot results for $x_1 < 0$. A perfect symmetry is observed in figures 3 and 4 between the downstroke and the upstroke, with $\Gamma_1 > 0$ for the downstroke (in our sign convection where Γ_1 is positive when clockwise) and $\Gamma_1 < 0$ during the upstroke.

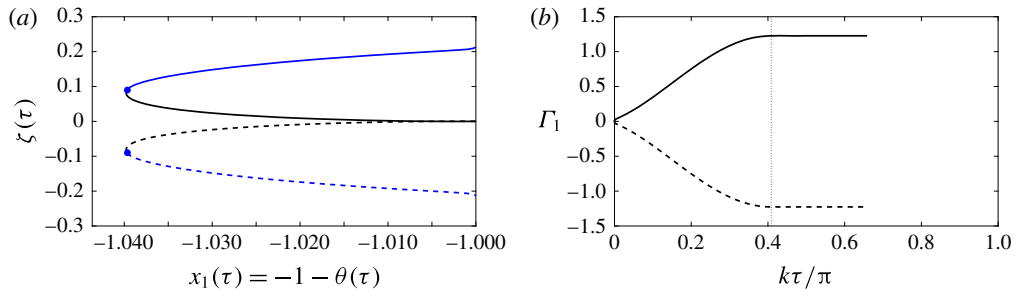

FIGURE 3. (Colour online) The LEV trajectory (*a*) and circulation (*b*) for $h_0 = 0.1$, $a_0 = 20°$, $a = 0$, $k = 5$ and $\phi = 10°$. The continuous lines correspond to the downstroke and the dashed lines to the upstroke. The circles in (*a*) mark the position at which Γ_1 reaches a maximum and the LEV is shed, whose instant is marked with a dotted vertical line in (*b*).

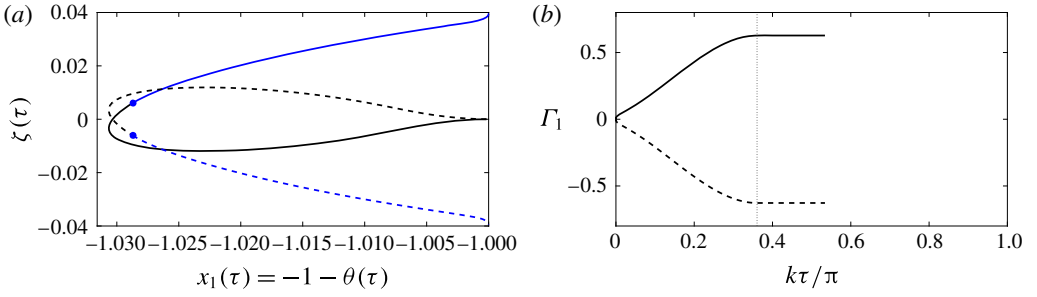

FIGURE 4. (Colour online) As figure 3, but for $\phi = 90°$.

For $h_0 = 0$, i.e. for a pure pitching motion, $\alpha_{i0} = \pm a_0$, $\alpha_{i1} = 0$, $\alpha_{i2} = \mp a_0 k^2/2$ and $z_{10} \simeq \pm a_0(1+a)(1-k^2\tau^2/2)$ according to the expressions given in appendix C. Thus, (4.32) yields, at the lowest order,

$$\theta \simeq [(1+a)a_0^2 k^2]^{2/3}\frac{\tau^{4/3}}{2}, \quad \zeta \simeq \pm\frac{3}{8}a_0 a k^2\tau^2, \quad \tau \ll 1, \tag{4.34a,b}$$

which have to be used to start the numerical integration of (4.29)–(4.30). Figure 5 shows results for this case when $a_0 = 20°$, $a = 0$ and $k = 5$. Comparing with figure 3, which is a similar case but with $h_0 = 0.1$, the maximum of Γ_1 and the largest $|\zeta|$ travelled by the vortex are both significantly smaller.

For $\sin\phi = 0$, i.e. for a combined motion without phase shift ($\phi = 0$), or with a phase shift $\phi = 180°$, $h_{i1} = \alpha_{i1} = 0$, $h_{i0} = \pm h_0$, $\alpha_{i0} = \pm a_0 \cos\phi$ from the expressions given in appendix C, where it has been taken into account that $\cos\phi = \pm 1$. At the lowest order, when $\tau \ll 1$, one obtains

$$\theta \simeq (k^2 a_0[(1+a)a_0 + h_0\cos\phi])^{2/3}\frac{\tau^{4/3}}{2}, \quad \zeta \simeq \pm\frac{3}{8}k^2(h_0 + a_0 a\cos\phi)\tau^2. \tag{4.35a,b}$$

Although this starting behaviour is very different from (4.33), the results as τ increases are quite similar in both cases for small ϕ or for ϕ close to 180°. For instance, the curves for $\phi = 0$ when $h_0 = 0.1$, $a_0 = 20°$, $a = 0$ and $k = 5$ are very similar to those

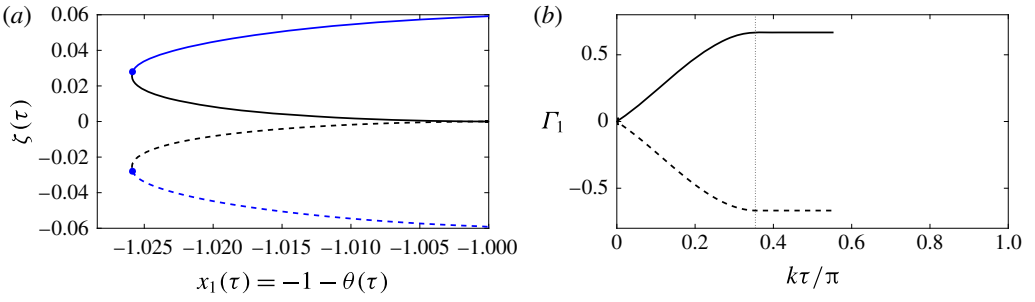

FIGURE 5. (Colour online) As figure 3, but for $h_0 = 0$.

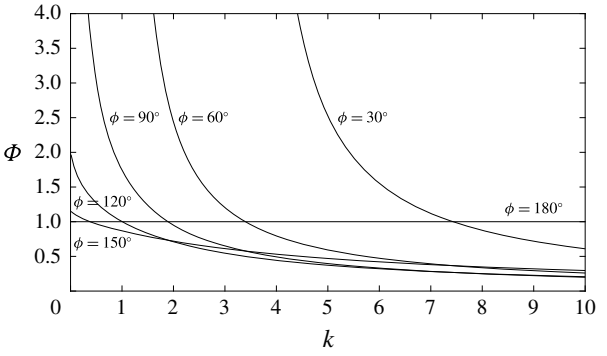

FIGURE 6. Plot of Φ, defined in (4.36), versus k for several values of ϕ.

depicted in figure 3 for $\phi = 10°$, except for very small τ. For this reason, these results are not plotted here.

Finally, for a pure heaving motion ($a_0 = 0$), the equations have no solution with the present approximation (4.28), which needs the presence of some pitching motion with $\dot{\alpha} \neq 0$ to generate an LEV. One would have to consider the next-order effects of ϖ_{11} in (4.6), but these second-order effects are neglected in the present approximation.

More generally, no LEV is produced within the present approximation when Γ_1 is negative at the beginning of the downstroke (or positive at the beginning of the upstroke), i.e. when $\mathcal{G}_{i0} = \mathcal{G}(\tau = 0) < 0$ for the downstroke (or $\mathcal{G}_{i0} > 0$ for the upstroke). From (C 3)–(C 8) in appendix C, this condition for the formation of the LEV can be written as

$$\frac{h_0}{(1+a)a_0} < \Phi(k,\phi) \equiv \frac{2F(k)}{k[3F(k)-1]\sin\phi - 2F(k)\cos\phi}, \tag{4.36}$$

valid for both the downstroke and the upstroke. This condition excludes the pure heaving motion already commented on, and allows any pure pitching motion ($h_0 = 0$) for any value of k or a. Any pitching of the foil pivoting at the leading edge ($a = -1$) is also excluded by this inequality.

Figure 6 shows Φ as a function of k for several values of ϕ. A solution exists, i.e. an LEV is generated, for values of k and $h_0/[(1+a)a_0]$ below the corresponding curve for a given phase shift ϕ. When ϕ is close to zero, the solution exists for practically any value of k and $h_0/[(1+a)a_0]$. However, as ϕ increases, the range

shrinks to smaller values of both parameters. If one starts to increase $h_0/[(1+a)a_0]$ (by decreasing the pitch angle a_0, say) for given values of k and $h_0/[(1+a)a_0]$ below the curve corresponding to a given value of the phase shift ϕ, what it is found is that τ_m decreases and the maximum circulation tends to zero as one approaches the curve, corresponding to a vanishing contribution of the LEV to the force and moment.

Condition (4.36) is the mathematical expression of the known physical condition that the effective angle of attack has to be sufficiently large for the flow to separate at the leading edge and develop an LEV that moves as a point vortex away from the edge (Dickinson & Götz 1993; Jones 2003; Xia & Mohseni 2013). It is a consequence of the Kutta condition imposed at the sharp leading edge while the LEV is growing. In fact, $\mathcal{G}(t)$, as defined in (4.24) proportional to the LEV circulation, is a measure of the average slip between the plate and the fluid adjacent to the plate (Jones 2003), which has to be positive at the beginning of the downstroke (negative for the upstroke) to generate an LEV that begins to move away from the plate. What it is remarkable here is that this condition can be written in terms of a single parameter $h_0/[(1+a)a_0]$ for given k and ϕ.

5. Results for the contribution of the LEV to the forces and moment

According to (3.7), (3.17) and (3.21), the contributions of the LEV with circulation $\Gamma_1(t)$ developed during each half-stroke to the lift, thrust and moment are given, in non-dimensional form, by

$$C_{L_1} = \frac{\mathrm{d}}{\mathrm{d}t}F_{L_1}, \quad F_{L_1} \equiv -\Gamma_1(x_1 + D_1), \tag{5.1}$$

$$C_{T_1} = \frac{\mathrm{d}}{\mathrm{d}t}F_{T_1}, \quad F_{T_1} \equiv \Gamma_1[z_s(x_1) - z_1 + \alpha(x_1 + D_1)], \tag{5.2}$$

$$C_{M_1} = \frac{\mathrm{d}}{\mathrm{d}t}F_{M_1}, \quad F_{M_1} \equiv \frac{1}{2}\Gamma_1\left[\frac{x_1^2}{2} + \frac{E_1}{2} - \frac{1}{4} - a(x_1 + D_1)\right], \tag{5.3}$$

where, as usual, the forces are scaled with $\rho U^2 c/2$ and the moment with $\rho U^2 c^2/2$. All of the magnitudes in these expressions are dimensionless (see (4.10)).

The quantities D_1 and E_1, which are integrals defined in (B 3) and (B 4) of appendix B respectively, are obtained in the present linear approximation by neglecting terms of order z_1^2,

$$D_1 \simeq -x_1 - \sqrt{x_1^2 - 1}, \quad E_1 \simeq \tfrac{1}{2} - x_1^2 - x_1\sqrt{x_1^2 - 1}, \quad \text{for} \quad x_1 \leqslant -1. \tag{5.4a,b}$$

They can also be obtained for $x_1 > -1$ with errors of $O(z_1^2)$. However, since we are considering only the effect of the growing LEV up to the point where its intensity $|\Gamma_1|$ reaches a maximum, and this maximum occurs in all significant cases for $x_1 \leqslant -1$ (see, e.g., figures 3–5), these expressions suffice in the present approximation. On substituting into (5.1)–(5.3), and using (4.14) and (4.24), one obtains

$$F_{L_1} = \Gamma_1\sqrt{x_1^2 - 1} \simeq 2\mathcal{G}\theta\left(1 + \frac{\theta}{4}\right), \tag{5.5}$$

$$F_{T_1} = \Gamma_1\left[z_s(x_1) - z_1 - \alpha\sqrt{x_1^2 - 1}\right] \simeq -2\mathcal{G}\theta\left[\zeta + \alpha\left(1 - \sqrt{\frac{\theta}{2}} + \frac{\theta}{4}\right)\right], \tag{5.6}$$

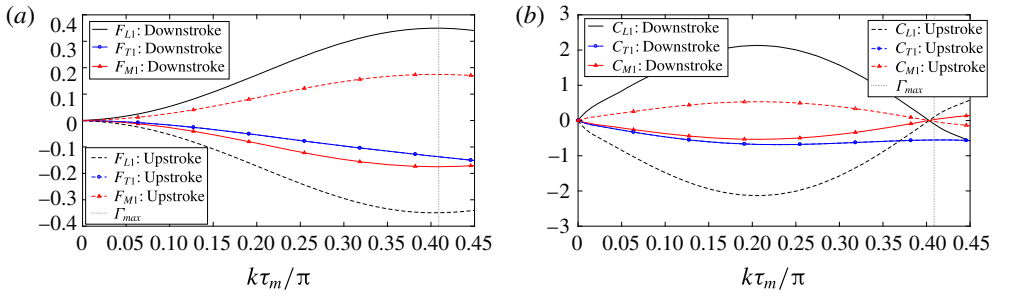

FIGURE 7. (Colour online) The functions (5.5)–(5.7) (*a*), and the force and moment coefficients (5.1)–(5.3) (*b*) for the case depicted in figure 3 ($h_0 = 0.1$, $a_0 = 20°$, $a = 0$, $k = 5$ and $\phi = 10°$), for both the downstroke (continuous lines) and the upstroke (dashed lines). The vertical dotted line marks the instant where $|\Gamma_1|$ reaches a maximum value.

$$F_{M_1} = \frac{1}{2}\Gamma_1\sqrt{x_1^2 - 1}\left(a - \frac{x_1}{2}\right) \simeq \mathcal{G}\theta\left[a + \frac{1}{2} + \frac{\theta}{4}\left(a + \frac{5}{2}\right)\right]. \tag{5.7}$$

It should be noted that we use the approximation $\theta \ll 1$, which is quite accurate in all of the cases considered (e.g. figures 3–5). At the initial stages of each half-stroke ($\tau \ll 1$), one may use (4.33) to find, at the leading order, $F_{L_1} \propto \tau^{2/3}$, $F_{T_1} \propto \tau^{4/3}$ and $F_{M_1} \propto \tau^{2/3}$, which yield, after using (5.1)–(5.3), the lift singularity at the start of the impulsive motion of a flat plate discussed by Graham (1983), $C_{L_1} \propto \tau^{-1/3}$, together with $C_{T_1} \propto \tau^{2/3}$ and $C_{M_1} \propto \tau^{-1/3}$.

These functions (5.5)–(5.7) are very relevant because, according to (5.1)–(5.3), their values up to a given instant τ within each half-stroke are proportional to the corresponding time-averaged force or moment up to that instant. Figure 7 shows F_{L_1}, F_{T_1} and F_{M_1}, as well as C_{L_1}, C_{T_1} and C_{M_1}, for the downstroke and the upstroke of a typical case (that of figure 3) up to the point where $|\Gamma_1|$ reaches a maximum. The main feature of this and all of the cases considered is that $C_{L_1}(\tau)$ and $C_{M_1}(\tau)$ for the upstroke are symmetrical in relation to the downstroke, so that the developing LEV does not contribute to the time-averaged lift and moment during a whole stroke. It only contributes to the instantaneous lift and moment, especially at the beginning of each half-stroke, by the contribution cancelling out with the next half-stroke. However, the evolution of $C_{T_1}(\tau)$ (and $F_{T_1}(\tau)$) for the upstroke coincides with its evolution during the downstroke. Thus, the growing LEV contributes to both the instantaneous thrust force and its time-averaged value. In addition, for most of the cases considered, the contribution to the time-averaged thrust is negative, i.e. the growing LEV generates drag in the mean, within the present approximation. This is consistent with the discussion on the general expression for T_j given in § 3, just below (3.17).

According to (5.2), the time-averaged thrust (actually drag in most cases) produced by the LEV during each half-stroke is given by the final value of the function F_{T_1} at the half-period $\tau = \pi/k$. However, since we are considering only the contribution of the LEV up to the instant τ_m where $|\Gamma_1|$ reaches a maximum value, the time-averaged thrust coefficient can be written as

$$\overline{C}_{T_1} \simeq \frac{2}{\tau_m}\int_0^{\tau_m} C_{T_1}\,\mathrm{d}\tau = \frac{2}{\tau_m}F_{T_1}(\tau = \tau_m), \tag{5.8}$$

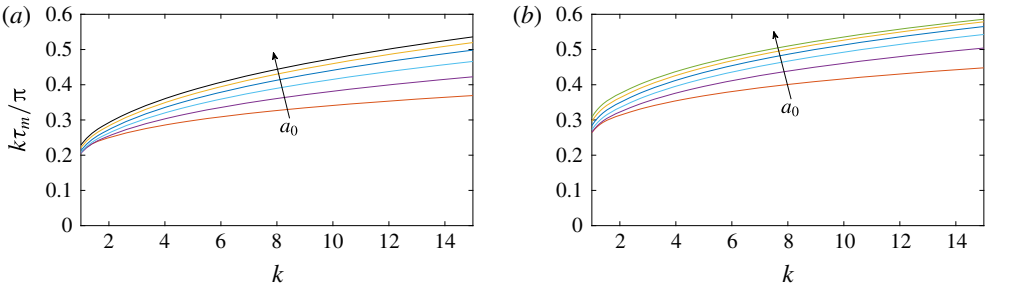

FIGURE 8. (Colour online) Plot of $k\tau_m/\pi$ versus k for a pure pitching motion with $a=0$ (a) and $a=0.5$ (b), and increasing values of a_0, from 10° (bottom curve) to 30° (top curve) with increments of 4°.

where it has been taken into account that $C_{T_1}(t)$ coincides for the downstroke and the upstroke, and that $F_{T_1}(\tau=0)=0$ (it should be remembered that $\tau=0$ corresponds to $t=t_i$ for each half-cycle). Thus, one has only to compute numerically the function F_{T_1} at $\tau=\tau_m$ from (5.6),

$$F_{T_1}(\tau=\tau_m)\simeq -2\mathcal{G}_m\theta_m\left[\zeta_m+\alpha_m\left(1-\sqrt{\frac{\theta_m}{2}+\frac{\theta_m}{4}}\right)\right], \tag{5.9}$$

where the subscript m means at $\tau=\tau_m$. Figure 8 shows $k\tau_m/\pi$, i.e. the fraction of each half-stroke during which $|\Gamma_1|$ increases, as a function of k for a pure pitching motion with several values of a_0 and two pitching axis locations. It is observed that $k\tau_m/\pi$ scales, approximately, as $(a_0k)^{1/4}$ for sufficiently large frequencies, with the proportionality constant slightly increasing with a.

Figure 9 shows $\overline{C}_{T_1}$ for a pure pitching motion as a function of the reduced frequency k for different values of the pitching amplitude a_0 and three values of the pitching axis location a. For small k and a_0, $|\overline{C}_{T_1}|$ is negligible, as expected. As commented on above, $\overline{C}_{T_1}$ is usually negative, i.e. the LEV produces drag in most cases within the present approximation. If this is the case, $\overline{C}_{T_1}$ is found to be roughly proportional to $-a_0^2k^3$ for sufficiently large k, with a proportionality constant that depends on a. This constant is significantly larger for $a=0.5$ than for $a=0$ (compare panels (a) and (b) in figure 9). Thus, the LEV correction to the thrust is more important when the pitching axis is downstream of the midchord point. For $a=-0.5$, $\overline{C}_{T_1}$ is positive and small for low a_0 and k (see the inset in figure 9c), being negative as in the other two cases for larger a_0 and k (it should be noted that the scale of $\overline{C}_{T_1}$ in figure 9(c) is not logarithmic to allow for this change of sign). For combined heaving and pitching motions that satisfy (4.36), it is found that $\overline{C}_{T_1}$ behaves in a similar fashion to the pure pitching motion in relation to k and a_0, with a weaker dependence on h_0 and ϕ.

6. Total time-averaged thrust and propulsion efficiency

From (3.14), the total time-averaged thrust coefficient is then

$$\overline{C}_T\simeq \overline{C}_{T_f}+\overline{C}_{T_1}, \tag{6.1}$$

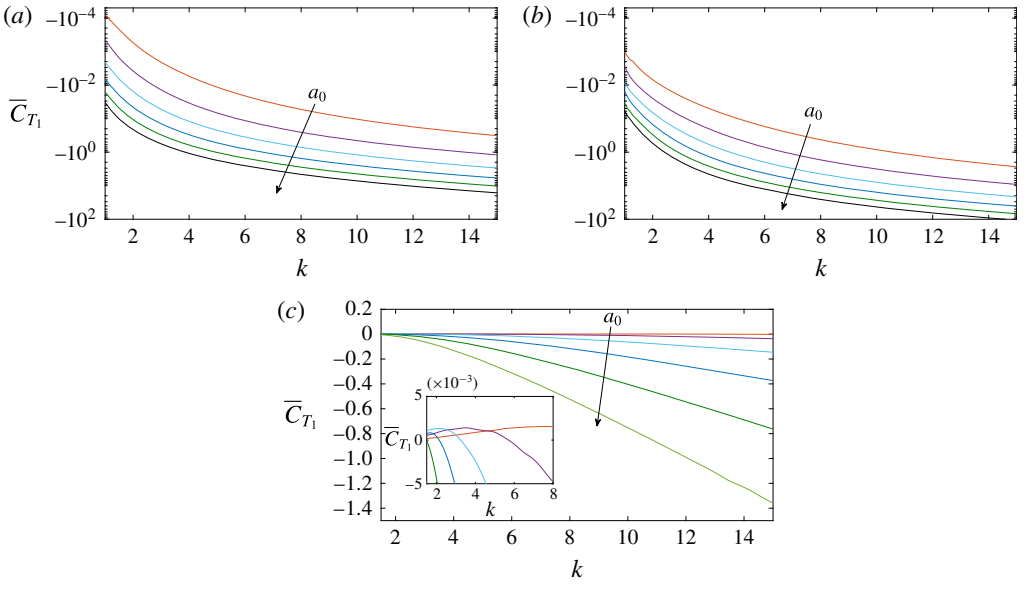

FIGURE 9. (Colour online) Plot of $\overline{C}_{T_1}$ versus k for a pure pitching motion for increasing values of a_0, from 10° (top curves) to 30° (bottom curves) with increments of 4°, for $a=0$ (*a*), $a=0.5$ (*b*) and $a=-0.5$ (*c*). (It should be remembered that the non-dimensional pivot axis ranges from $a=-1$ at the leading edge to $a=1$ at the trailing edge.)

where $\overline{C}_{T_f} \equiv \overline{C}_{T_a} + \overline{C}_{T_e}$ is the sum of the time-averaged values of the non-dimensional forms of T_a and T_e given by (3.15)–(3.16) over a whole stroke of period $2\pi/k$ (the subscript f is for 'free' of leading-edge, or any other point, vortex). The expression for $\overline{C}_{T_f}$ as a function of k, h_0, a_0, a and ϕ can be found in Fernandez-Feria (2016, 2017), which modifies previous expressions by Garrick (1936).

Of particular interest in forward flight flapping aerodynamics is the time-average propulsion efficiency, defined as

$$\eta = \frac{\overline{C}_T}{\overline{C}_P}, \tag{6.2}$$

where $\overline{C}_P$ is the time-averaged power coefficient, given by the lift force times heave velocity plus the pitching moment times pitch angular velocity,

$$\overline{C}_P = -\overline{C_L \dot{h}} - \overline{C_M \dot{\alpha}}. \tag{6.3}$$

It must be noted that, although the LEV does not contribute to the averaged lift and moment in the present approximation, i.e. $\overline{C}_{L_1} = \overline{C}_{M_1} = 0$, so that $\overline{C}_L = \overline{C}_{L_f} \equiv \overline{C}_{L_a} + \overline{C}_{L_e}$, with C_{L_a} and C_{L_e} the non-dimensional forms of L_a and L_e given in (3.5)–(3.6), and similarly for the moment with M_a and M_e given by (3.19)–(3.20), the LEV does contribute to the averaged input power coefficient because it comes from the time averaging of the products in (6.3). By writing

$$\overline{C}_{P_f} \equiv -\overline{C_{L_f} \dot{h}} - \overline{C_{M_f} \dot{\alpha}}, \tag{6.4}$$

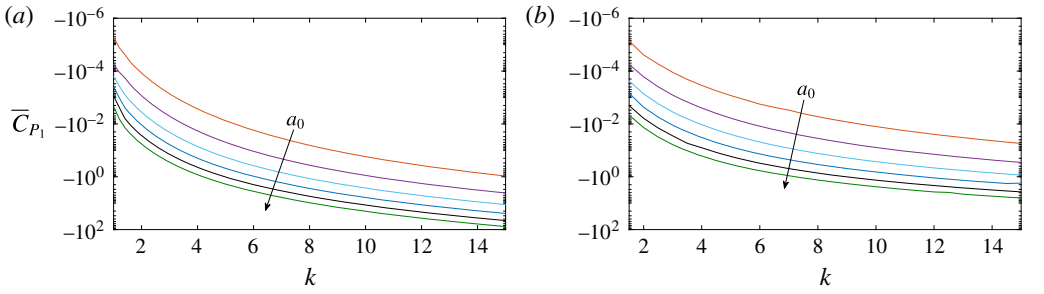

FIGURE 10. (Colour online) Plot of $\overline{C}_{P_1}$ versus k for a pure pitching motion for increasing values of a_0, from 10° (top curves) to 30° (bottom curves) with increments of 4°, for $a=0$ (*a*) and $a=-0.5$ (*b*).

averaged over the whole period $2\pi/k$, and

$$\overline{C}_{P_1} \equiv -\overline{C_{L_1}\dot{h}} - \overline{C_{M_1}\dot{\alpha}} \simeq -\frac{2}{\tau_m}\int_0^{\tau_m} (C_{L_1}\dot{h} + C_{M_1}\dot{\alpha})\,\mathrm{d}\tau, \tag{6.5}$$

(6.3) can be written as

$$\overline{C}_P \simeq \overline{C}_{P_f} + \overline{C}_{P_1}. \tag{6.6}$$

Closed expressions for $\overline{C}_{P_f}$ in terms of k, h_0, a_0, a and ϕ were originally derived by Theodorsen (1935) and Garrick (1936) and can be found in many references. To obtain $\overline{C}_{P_1}$, one has to use the expressions (5.1) and (5.3) for C_{L_1} and C_{M_1} in (6.5). Alternatively, by integrating by parts, it can be written in terms of F_{L_1} and F_{M_1} as

$$\overline{C}_{P_1} \simeq \frac{2}{\tau_m}\left[\int_0^{\tau_m} (F_{L_1}\ddot{h} + F_{M_1}\ddot{\alpha})\,\mathrm{d}\tau - (F_{L_1}\dot{h} + F_{M_1}\dot{\alpha})_{\tau=\tau_m}\right]. \tag{6.7}$$

Figure 10 shows $\overline{C}_{P_1}$ for a pitching motion versus the reduced frequency k for different values of the pitching amplitude a_0 and two values of the pitching axis location a. For large k, $|\overline{C}_{P_1}|$ is approximately proportional to $a_0^4 k^3$, with the proportionality constant increasing with a. As in the case of $\overline{C}_{T_1}$ (figure 9), the effect of the LEV is larger for a pivot location downstream of the midchord point ($a>0$), especially as a_0 and k increase.

7. Comparison with experimental results

Here, we first compare the above theoretical results with the recent experimental data for a pitching foil reported by Mackowski & Williamson (2017). These authors measured $\overline{C}_T$ and η directly for different pivot point locations and several values of the reduced frequency at a Reynolds number of 17 000. To account for the viscous effects, especially relevant at low frequencies, we add a quasisteady thrust coefficient $C_{T_0}<0$ (actually a drag coefficient), which was experimentally computed by these authors by averaging the airfoil static drag over the pitch angles encountered during a cycle of oscillation. By adding this C_{T_0} to $\overline{C}_T$, the results of the potential theory based on the vortical impulse agree quite well with experimental data for sufficiently small

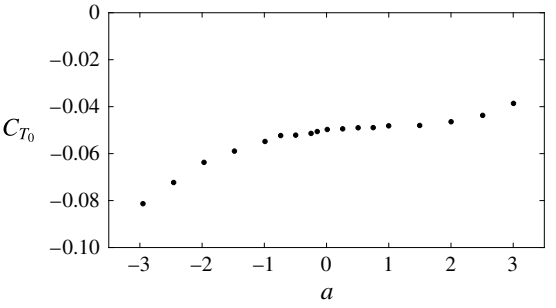

FIGURE 11. Quasisteady drag C_{T_0} versus a measured by Mackowski & Williamson (2017) for an NACA 0012 foil at $Re = 17\,000$ for $a_0 = 8°$. It should be remembered that $-1 \leqslant a \leqslant 1$ for a pivot location inside the foil.

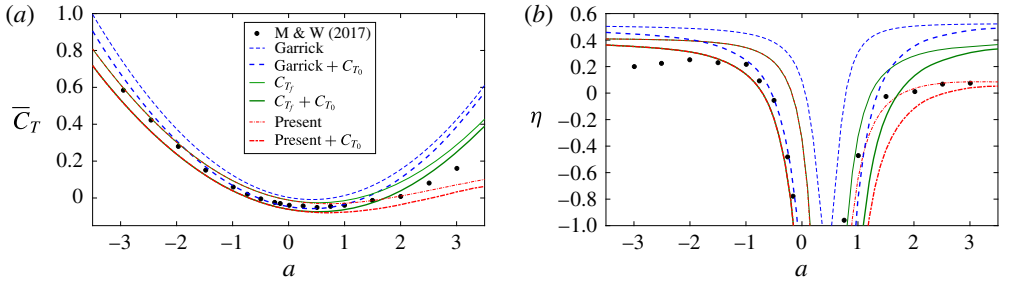

FIGURE 12. (Colour online) Comparison of the experimental data of Mackowski & Williamson (2017) for $\overline{C}_T$ (a) and η (b) versus a for $k = 2$ and $a_0 = 8°$ (dots, from figures 6 and 7 of Mackowski and Williamson) with the present results (dashed and dotted lines), with the results without the LEV effect (continuous lines) and with Garrick's (1936) results (dashed lines). The different theoretical results are presented in two ways, adding the experimental value of $C_{T_0}(a)$ given in figure 11 to $\overline{C}_T$, and without adding it.

amplitude of the oscillations (Fernandez-Feria 2017). This C_{T_0} depends, for a pitching foil, on the maximum pitch angle a_0 and the pivot location a. Figure 11 shows the measured values for $a_0 = 8°$ as a function of a.

Figure 12 compares the experimental results for the thrust coefficient and propulsive efficiency obtained by Mackowski & Williamson (2017) for $k = 2$, $a_0 = 8°$ and different values of the pivot location a with the present results for $\overline{C}_T$ and η. Also included are the results obtained without considering the LEV effect, i.e. $\overline{C}_{T_f}$ and $\eta_f \equiv \overline{C}_{T_f}/\overline{C}_{P_f}$, as well as Garrick's (1936) results for $\overline{C}_T$ and η. The theoretical results are presented in two ways: with the addition of the quasisteady constant drag $\overline{C}_{T_0}(a)$, as given in figure 11, to correct $\overline{C}_T$, and also without adding the experimentally based $\overline{C}_{T_0}(a)$. The main feature arising from this figure is that the LEV effect is relevant, within the present approximation, when $a > 0$: the LEV corrections to $\overline{C}_T$ and η are negligible when the pivot location is ahead of the midchord point ($a < 0$), while they are increasingly important as the pivot point approaches the trailing edge or is located further downstream. The differences between Garrick's classical results and the present ones based on the vortical impulse theory are also more pronounced in these cases with $a > 0$. The correction provided by this theory, already discussed in

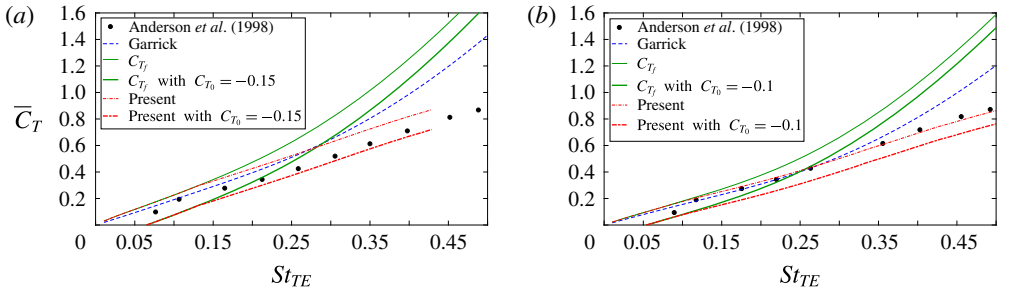

FIGURE 13. (Colour online) Comparison of the theoretical results with the experimental data of Anderson *et al.* (1998) for $\overline{C}_T$ versus the Strouhal number based on the total excursion of the trailing edge, St_{TE}, for a combined plunging and pitching motion of an NACA 0012 airfoil with $a = -1/3$ in two cases: $h_0 = 1.5$, $\alpha_{max} = 21°$, $\phi = 75°$ (case 1 from figure 1 of Anderson *et al.*) (*a*) and $h_0 = 1.5$, $\alpha_0 = 15°$, $\phi = 75°$ (from figure 9*a* of Anderson *et al.*) (*b*). The theoretical results are presented adding a constant quasisteady drag C_{T_0} to $\overline{C}_T$, given in the legend (estimated from Mackowski & Williamson (2017) for a similar amplitude), and also without adding it.

Fernandez-Feria (2016), is here increased when the LEV effect is taken into account, so that the agreement of the present propulsive efficiency with the experimental data is overall better for all pivot locations.

Figure 13 compares the theoretical results with the experimental data for $\overline{C}_T$ obtained by Anderson *et al.* (1998) for a combined pitching and plunging motion in two of the optimal cases where experiment provides very high efficiency for an NACA 0012 airfoil pivoting at one-third-chord point. These two cases, both with $\phi = 75°$, are among the few of those reported by Anderson *et al.* (1998) that satisfy the condition (4.36). It is observed that the agreement with the experimental data improves when the present LEV effect is taken into account, almost independently of whether we add, or not, a constant quasisteady drag C_{T_0}, which has to be estimated from experimental data.

8. Conclusion

We have developed general expressions for the contribution of travelling point vortices to the lift, thrust, moment and propulsion efficiency of a two-dimensional pitching and heaving airfoil from a vortical impulse formulation within the linear potential theory. Although these general formulae need additional information about the temporal evolution of the vortices, both circulation and trajectory, they provide useful qualitative information about their effect on the airfoil unsteady aerodynamics.

Starting from these general formulae, we have derived closed-form expressions for the LEV contribution to the unsteady forces and moment on the airfoil. To that end, we have used several simplifying assumptions for the development and shedding of the LEV. We have considered only one point vortex during each half-stroke, an LEV that is released from the sharp leading edge where one can apply the unsteady Kutta condition that regularizes the bound vortex-sheet strength at the leading edge, and used the Brown–Michael equation for the developing LEV, which ensures momentum conservation. With these assumptions, the symmetry of the problem shows that the LEV does not contribute to the time-averaged lift and moment, but only to the time-averaged thrust and the propulsion efficiency, which are in general lowered in relation

to the case without LEV. Further, by considering the effect of the developing LEV just up to its shedding point, when its circulation reaches an extremum value according to the Brown–Michael model, we are able to obtain quite simple relations for the LEV effect on the thrust force and propulsion efficiency, which constitutes a lowest-order correction to the analytical results from the linear potential theory. The resulting thrust coefficient and propulsion efficiency corrected by the LEV agree reasonably well with recent experimental results for a foil pitching at different pivot locations when the pitching amplitude is small enough for the linear theory to be valid.

As a general trend, it is found that the LEV lowest-order corrections to the thrust force and propulsion efficiency are more significant when the pitching axis location is behind the midchord point ($a > 0$), the more so the larger the pitching amplitude and the reduced frequency are. These are, in fact, the conditions where the classical Garrick expressions for the thrust and efficiency are in greater disagreement with experimental results for a pure pitching motion. In addition, no LEV corrections are found within the present linear approximation for a pure heaving motion ($a_0 = 0$), or, more generally, when $h_0/(1+a)a_0$ is larger than a quantity that depends on k and ϕ.

The present contribution of the effect of the LEV on the unsteady aerodynamics of a two-dimensional airfoil is limited to thin rigid airfoils with small-to-medium angles of attack. It may complement the large amount of information already existing in the literature about the LEV effect on the unsteady aerodynamics of flapping wings in a great variety of kinematics and flow conditions. We provide closed-form corrections to the very useful and long-time used analytical expressions from the linear potential theory. Better approximations can be obtained from more complete models for the development and shedding of the LEV, but at the cost of more parameters to be adjusted experimentally and probably not in a closed simple form.

Acknowledgements

This research has been supported by the Ministerio de Economía y Competitividad of Spain grant nos DPI2013-40479-P and DPI2016-76151-C2-1-R.

Appendix A. A note on the Kutta condition at the trailing edge and the general validity of (2.26)–(2.27)

In § 2.2, we applied the Kutta condition at the trailing edge separately to each component of ϖ_s defined in (2.13), satisfying the integral equations (2.17)–(2.19). However, in fact, it has to be applied just once to the whole vorticity distribution on the foil, which has to be regular at $x = 1$. In doing this, the following relation results for the circulations Γ_0, Γ_{1e} and Γ_{1j} of the components of ϖ_s, which are arbitrary 'constants' from the integral equations (2.17)–(2.19):

$$\Gamma_0(t) + \Gamma_{1e}(t) + \sum_{j=1}^{N} \Gamma_{1j}(t) = -2 \fint_{-1}^{1} \sqrt{\frac{1+\xi}{1-\xi}}\, v_0(\xi, t)\, \mathrm{d}\xi + \int_1^{\infty} \left(\sqrt{\frac{\xi+1}{\xi-1}} - 1 \right) \varpi_e(\xi, t)\, \mathrm{d}\xi + \sum_{j=1}^{N} \Gamma_j(t) C_j(t), \tag{A 1}$$

where the $C_j(t)$ are given by (2.25) in terms of $\Gamma_j(t)$ and $[x_j(t), z_j(t)]$. On substituting into (2.13), one obtains the same vorticity distribution (2.27), but without identifying

$\Gamma_0(t)$ with the first term on the right-hand side of (A 1), Γ_{1e} with the second term, and so on. Moreover, on substituting into Kelvin's theorem (2.15), one obtains

$$\int_1^\infty \sqrt{\frac{\xi+1}{\xi-1}}\varpi_e(\xi,t)\,\mathrm{d}\xi = 2\fint_{-1}^1 \sqrt{\frac{1+\xi}{1-\xi}}v_0(\xi,t)\,\mathrm{d}\xi - \sum_{j=1}^N \Gamma_j(t)[1+C_j(t)], \quad \text{(A 2)}$$

which, again, is the same as (2.26) if the first term on the right-hand side is called $-\Gamma_0(t)$. Therefore, since the force and moment on the foil depend only on the vorticity distributions $\varpi_s(x,t)$ and $\varpi_e(x,t)$, the same expressions are obtained if we apply the Kutta condition at the trailing edge to the whole vorticity distribution ϖ_s, or independently to each of its components in which we have separated ϖ_s, which is a consequence of the linearity of the problem.

The purely formal advantage of denoting the first term on the right-hand side of (A 1) as $\Gamma_0(t)$, i.e. of using (2.24), is that $\Gamma_0(t)$ corresponds to the quasisteady bound circulation around the foil in the absence of unsteady trailing wake and point vortices, as cleverly shown by von Kármán & Sears (1938). Thus, it is also useful to denote the second term on the right-hand side of (A 1) as Γ_{1e} and the N terms associated with Γ_j on the right-hand side of (A 1) as Γ_{1j}, as done in (2.21) and (2.25) respectively.

Appendix B. Some integrals involving ϖ_s

To compute (2.8), (2.9) and (2.12), one needs several moments of ϖ_s (i.e. of ϖ_0, ϖ_{1j} and ϖ_{1e}),

$$\fint_{-1}^1 x\varpi_0(x,t)\,\mathrm{d}x = \pi(\dot h + a\dot\alpha - U\alpha) = \frac{1}{2}(\pi\dot\alpha - \Gamma_0), \quad \text{(B 1)}$$

$$\fint_{-1}^1 x^2\varpi_0(x,t)\,\mathrm{d}x = \frac{\Gamma_0}{2} - \frac{\pi}{4}\dot\alpha = \pi\left[U\alpha - \dot h - \left(a-\frac{1}{4}\right)\dot\alpha\right], \quad \text{(B 2)}$$

$$\fint_{-1}^1 x\varpi_{1j}(x,t)\,\mathrm{d}x = D_j(t)\Gamma_j(t), \quad D_j \equiv \frac{1}{\pi}\fint_{-1}^1 \sqrt{1-\xi^2}\,\frac{\xi - x_j}{(\xi-x_j)^2+z_j^2}\,\mathrm{d}\xi, \quad \text{(B 3}a,b\text{)}$$

$$\fint_{-1}^1 x^2\varpi_{1j}(x,t)\,\mathrm{d}x = \left[\frac{C_j(t)}{2} + E_j(t)\right]\Gamma_j(t), \quad E_j \equiv \frac{1}{\pi}\fint_{-1}^1 \xi\sqrt{1-\xi^2}\,\frac{\xi - x_j}{(\xi-x_j)^2+z_j^2}\,\mathrm{d}\xi, \quad \text{(B 4}a,b\text{)}$$

$$\fint_{-1}^1 x\varpi_{1e}(x,t)\,\mathrm{d}x = \int_1^\infty (\sqrt{\xi^2-1} - \xi)\varpi_e(\xi,t)\,\mathrm{d}\xi, \quad \text{(B 5)}$$

$$\fint_{-1}^1 x^2\varpi_{1e}(x,t)\,\mathrm{d}x = \int_1^\infty \left(\frac{1}{2}\sqrt{\frac{\xi+1}{\xi-1}} + \xi\sqrt{\xi^2-1} - \xi^2\right)\varpi_e(\xi,t)\,\mathrm{d}\xi. \quad \text{(B 6)}$$

Appendix C. The terms $h(\tau)$, $\alpha(\tau)$, $z_{10}(\tau)$ and $\mathcal{G}(\tau)$ for $\tau \ll 1$

For $\tau \ll 1$, one may write

$$h \simeq h_{i0} + h_{i1}\tau + h_{i2}\tau^2, \quad \alpha \simeq \alpha_{i0} + \alpha_{i1}\tau + \alpha_{i2}\tau^2, \quad \text{(C 1}a,b\text{)}$$

with h_{i0} and α_{i0} the values of h and α at $t = t_i$ respectively and

$$h_{i1} + (1+a)\alpha_{i1} = 0 \tag{C 2}$$

to satisfy (4.9) at $\tau = 0$. From (4.11), one obtains, after some algebra,

$$h_{i0} = \frac{\pm h_0[h_0 + (1+a)a_0\cos\phi]}{[h_0^2 + (1+a)^2a_0^2 + 2h_0a_0(1+a)\cos\phi]^{1/2}}, \tag{C 3}$$

$$h_{i1} = \frac{\pm k h_0(1+a)a_0\sin\phi}{[h_0^2 + (1+a)^2a_0^2 + 2h_0a_0(1+a)\cos\phi]^{1/2}}, \quad h_{12} = -\frac{k^2}{2}h_{i0}, \tag{C 4a,b}$$

$$\alpha_{i0} = \frac{\pm a_0[h_0\cos\phi + (1+a)a_0]}{[h_0^2 + (1+a)^2a_0^2 + 2h_0a_0(1+a)\cos\phi]^{1/2}}, \quad \alpha_{i1} = -\frac{h_{i1}}{1+a}, \quad \alpha_{i2} = -\frac{k^2}{2}\alpha_{i0}, \tag{C 5a–c}$$

where the upper sign is for the downstroke and the lower sign for the upstroke. On the other hand,

$$z_{10} \simeq h_{i0} + (1+a)\alpha_{i0} + [h_{i2} + (1+a)\alpha_{i2}]\tau^2 \equiv z_{100} + z_{102}\tau^2 \tag{C 6}$$

and

$$\mathcal{G} \simeq \mathcal{G}_{i0} + \mathcal{G}_{i1}\tau, \tag{C 7}$$

with

$$\mathcal{G}_{i0} = 2\pi\left[\alpha_{i0} - h_{i1} - \left(a - \tfrac{1}{2}\right)\alpha_{i1}\right]F(k) - \pi\alpha_{i1}, \tag{C 8}$$

$$\mathcal{G}_{i1} = 2\pi\left[\alpha_{i1} - h_{i2} - \left(a - \tfrac{1}{2}\right)\alpha_{i2}\right]F(k) - 2\pi\alpha_{i2}. \tag{C 9}$$

REFERENCES

ALAMINOS-QUESADA, J. & FERNANDEZ-FERIA, R. 2017 Effect of the angle of attack on the transient lift during the interaction of a vortex with a flat plate: potential theory and experimental results. *J. Fluids Struct.* **74**, 130–141.

ANDERSON, J. M., STREITLIEN, K., BARRET, K. S. & TRIANTAFYLLOU, M. S 1998 Oscillating foils of high propulsive efficiency. *J. Fluid Mech.* **360**, 41–72.

BAIK, Y. S., BERNAL, L. P., GRANLUND, K. & OL, M. V. 2012 Unsteady force generation and vortex dynamics of pitching and plunging aerofoils. *J. Fluid Mech.* **709**, 37–68.

BROWN, C. E. & MICHAEL, W. H. 1954 Effect of leading edge separation on the lift of a delta wing. *J. Aero. Sci.* **21**, 690–694.

CARRIER, G. F., KROOK, M. & PEARSON, C. E. 2005 *Functions of a Complex Variable. Theory and Technique*. SIAM.

CORDES, U., KAMPERS, G., MEISSNER, T., TROPEA, C., PINKE, J. & HÖLLING, M. 2017 Note on the limitations of the Theodorsen and Sears functions. *J. Fluid Mech.* **811**, R1.

DICKINSON, M. H. & GÖTZ, K. G. 1993 Unsteady aerodynamics performance of model wings at low Reynolds numbers. *J. Exp. Biol.* **174**, 45–64.

ELLINGTON, C. P. 1984 The aerodynamics of hovering insect flight. Part IV. Aeorodynamic mechanisms. *Phil. Trans. R. Soc. Lond.* B **305**, 79–113.

ELLINGTON, C. P., VAN DEN BERG, C., WILLMOTT, A. P. & THOMAS, A. L. R. 1996 Leading-edge vortices in insect flight. *Nature* **384**, 626–630.

FERNANDEZ-FERIA, R. 2016 Linearized propulsion theory of flapping airfoils revisited. *Phys. Rev. Fluids* **1**, 084502.

FERNANDEZ-FERIA, R. 2017 Note on optimum propulsion of heaving and pitching airfoils from linear potential theory. *J. Fluid Mech.* **826**, 781–796.

GARRICK, I. E. 1936 Propulsion of a flapping and oscillating airfoil. NACA *Tech. Rep.* TR 567.

GARRICK, I. E. 1938 On some reciprocal relations in the theory of nonstationary flows. NACA *Tech. Rep.* TR 629.

GRAHAM, J. M. R. 1983 The lift on an aerofoil in starting flow. *J. Fluid Mech.* **133**, 413–425.

GRAHAM, W. R., PITT FORD, C. W. & BABINSKY, H. 2017 An impulse-based approach to estimating forces in unsteady flow. *J. Fluid Mech.* **815**, 60–76.

HEMATI, M. S., ELDREDGE, J. D. & SPEYER, J. L. 2014 Improving vortex models via optimal control theory. *J. Fluids Struct.* **49**, 91–111.

HOWE, M. S. 1996 Emendation of the Brown and Michael equation, with application to sound generation by vortex motion near a half-plane. *J. Fluid Mech.* **329**, 89–101.

JONES, M. A. 2003 The separated flow of an inviscid fluid around a moving flat plate. *J. Fluid Mech.* **496**, 405–441.

VON KÁRMÁN, T. & SEARS, W. R. 1938 Airfoil theory for non-uniform motion. *J. Aero. Sci.* **5**, 370–390.

LI, J., BAI, C.-Y. & WU, Z.-N. 2015 A two-dimensional multibody integral approach for forces in inviscid flow with free vortices and vortex production. *J. Fluids Engng* **137**, 021205.

LI, J. & WU, Z. N. 2015 Unsteady lift for the Wagner problem in the presence of additional leading/trailing edge vortices. *J. Fluid Mech.* **769**, 182–217.

LI, J. & WU, Z. N. 2016 A vortex force study for a flat plate at high angle of attack. *J. Fluid Mech.* **801**, 222–249.

MACKOWSKI, A. W. & WILLIAMSON, H. K. 2015 Direct measurement of thrust and efficiency of an airfoil undergoing pure pitching. *J. Fluid Mech.* **765**, 524–543.

MACKOWSKI, A. W. & WILLIAMSON, H. K. 2017 Effect of pivot point location and passive heave on propulsion from a pitching airfoil. *Phys. Rev. Fluids* **2**, 013101.

MARTÍN-ALCÁNTARA, A., FERNANDEZ-FERIA, R. & SANMIGUEL-ROJAS, E. 2015 Vortex flow structures and interactions for the optimum thrust efficiency of a heaving airfoil at different mean angles of attack. *Phys. Fluids* **27**, 073602.

MAXWORTHY, T. 2007 The formation and maintenance of a leading-edge vortex during the forward motion of an animal wing. *J. Fluid Mech.* **587**, 471–475.

MCGOWAN, G. Z., GRANLUND, K., OL, M. V., GOPALARATHNAM, A. & EDWARDS, J. R. 2011 Investigations of lift-based pitch–plunge equivalence for airfoils at low Reynolds numbers. *AIAA J.* **49**, 1511–1524.

MICHELIN, S. & LLEWELLYN SMITH, S. G. 2009 An unsteady point vortex method for coupled fluid–solid problems. *Theor. Comput. Fluid Dyn.* **23**, 127–153.

MINOTTI, F. O. 2002 Unsteady two-dimensional theory of a flapping wing. *Phys. Rev.* E **66**, 051907.

NEWMAN, J. N. 1977 *Marine Hydrodynamics*. MIT Press.

OLVER, F. W. J. & MAXIMON, L. C. 2010 Bessel functions. In *NIST Handbook of Mathematical Functions* (ed. F. W. J. Olver, D. W. Lozier, R. F. Boisvert & C. W. Clark), pp. 215–286. National Institute of Standards and Technology.

PITT FORD, C. W. & BABINSKY, H. 2013 Lift and the leading-edge vortex. *J. Fluid Mech.* **720**, 280–313.

PULLIN, D. I. & WANG, Z. J. 2004 Unsteady forces on an accelerating plate and application to hovering insect flight. *J. Fluid Mech.* **509**, 1–21.

RAMESH, K., GOPALARATHNAM, A., EDWARDS, J. R., OL, M. V. & GRANLUND, K. 2013 An unsteady airfoil theory applied to pitching motions validated against experiment and computation. *Theor. Comput. Fluid Dyn.* **27**, 843–864.

SAFFMAN, P. G. 1992 *Vortex Dynamics*. Cambridge University Press.

SHYY, W. & LIU, H. 2007 Flapping wings and aerodynamic lift: the role of the leading-edge vortex. *AIAA J.* **45**, 2817–2819.

TCHIEU, A. A. & LEONARD, A. 2011 A discrete-vortex model for the arbitrary motion of a thin airfoil with fluidic control. *J. Fluids Struct.* **27**, 680–693.

THEODORSEN, T. 1935 General theory of aerodynamic instability and the mechanism of flutter. NACA *Tech. Rep.* TR 496.

WANG, C. & ELDREDGE, J. D. 2013 Low-order phenomenological modeling of leading-edge vortex formation. *Theor. Comput. Fluid Dyn.* **27**, 577–598.

WANG, Z. J. 2000 Vortex shedding and frequency selection in flapping fight. *J. Fluid Mech.* **410**, 323–341.

WANG, Z. J. 2005 Dissecting insect flight. *Annu. Rev. Fluid Mech.* **37**, 183–210.

WU, J. C. 1981 Theory for the aerodynamic force and moment in viscous flows. *AIAA J.* **19**, 432–441.

WU, J.-Z., MA, H.-Y. & ZHOU, M.-D. 2006 *Vorticity and Vortex Dynamics*. Springer.

XIA, X. & MOHSENI, K. 2013 Lift evaluation of a two-dimensional pitching flat plate. *Phys. Fluids* **25**, 091901.

XIA, X. & MOHSENI, K. 2017 Unsteady aerodynamics of vortex-sheet formulation of a two-dimensional airfoil. *J. Fluid Mech.* **830**, 439–478.